

N 8 2 - 3 1 2 9 8



NASA Contractor Report 165896

NASA-CR-165896
19820023422

Aeroelastic Analysis for Helicopter Rotors With Blade Appended Pendulum Vibration Absorbers — Mathematical Derivations and Program User's Manual

Richard L. Bielawa

UNITED TECHNOLOGIES RESEARCH CENTER
East Hartford, CT 06108

Contract NAS1-16058
June 1982



National Aeronautics and
Space Administration

Langley Research Center
Hampton, Virginia 23665
AC 804 827-3966



PREFACE

The G400PA mathematical formulations and resulting computer code described herein were developed by United Technologies Research Center (UTRC) under Contract NAS1-16058, "Coupled Rotor Fuselage Vibration Analysis". This contract was through the Structures Laboratory of the USRTL (AVRADCOM) and Sikorsky Aircraft Division of the United Technologies Corporation was prime contractor. The initial development of the G400 analysis was conducted at UTRC by Dr. Richard L. Bielawa under Corporate sponsored independent research and development. Extensive refinements to the analysis were made under sponsorship of the Langley Research Center of the National Aeronautics and Space Administration and the U.S. Army Air Mobility Research and Development Laboratory, Langley Directorate as part of Contract NAS1-10960. This effort constitutes one of the contributing technologies to the Simplified Coupled Rotor Fuselage Vibration Analysis (SIMVIB) also funded through Contract NAS1-16058.

Aeroelastic Analysis for Helicopter Rotors With
Blade Appended Pendulum Vibration Absorbers-
Mathematical Derivatives and Program

TABLE OF CONTENTS

	Page
PREFACE	iii
LIST OF FIGURES AND TABLES.	vii
SUMMARY	1
INTRODUCTION.	3
LIST OF SYMBOLS	5
SIMULATION OF UNDERSLUNG TEETERED ROTORS.	11
Basic Modeling Considerations	11
Aerodynamic and Dynamic Load Distributions	12
Implementation of Teetered Blade Root Constraint	14
Teeter Stop Moment Characteristics	15
BLADE APPENDED PENDULUM VIBRATION ABSORBERS	19
Basic Assumptions	19
Dynamic Loads	21
Equations of Motion	22
BLADE LOADS DUE TO HIGHER HARMONIC EXCITATIONS.	25
Prescribed Harmonic Hub Motions	25
Higher Harmonic Blade Pitch Control.	31
Impedance Matrix Calculation	32
GENERAL DESCRIPTION OF THE G400PA PROGRAM STRUCTURE	33
Program Structure	33
Brief Description of Program Elements.	36

TABLE OF CONTENTS (Cont'd)

	Page
PROGRAM INPUT DESCRIPTION	43
Airfoil Data	43
Inertia, Elastic, Geometric and Other Operation Data	46
Blade Mode Shape Data	68
Multiple Case Runs	70
General Information to Facilitate Operation and Improve Efficiency	72
PROGRAM OUTPUT DESCRIPTION	77
Listing of Input Data	77
Parameters Calculated from Input Data	77
Results of Time-History Solution	84
Impedance Matrices	96
REFERENCES	99
APPENDICES: I: UPDATES TO DOCUMENTATION OF BASIC G400 ANALYSIS . .	101

FIGURES	Page
1. Schematic of Teetered Rotor System - Kinematic Definitions and Flapping Moment Equilibrium	13
2. Generalization of Nonlinear Teeter Stop Moment vs. Teeter Angle Characteristics	17
3. Pictorial of Typical Pendular Absorber Installation	20
4. Blade Trailing Edge View of Blade/Pendular Absorber System- Kinematic Definitions and Moment Equilibrium	23

TABLES	
I. Hierarchical Listing of G400PA Elements	34
II. Summary of Optional Basic Trim Combinations	74

Aeroelastic Analysis for Helicopter Rotors
with Blade Appended Pendulum Vibration Absorbers -
Mathematical Derivations and Program User's Manual^{*}

by

Richard L. Bielawa
United Technologies Research Center

SUMMARY

Mathematical development is presented for the expanded capabilities of the United Technologies Research Center (UTRC) G400 Rotor Aeroelastic Analysis. This expanded analysis, G400PA, simulates the dynamics of teetered rotors, blade pendulum vibration absorbers and the higher harmonic excitations resulting from prescribed vibratory hub motions and higher harmonic blade pitch control. Formulations are also presented for calculating the rotor impedance matrix appropriate to these higher harmonic blade excitations. This impedance matrix and the associated vibratory hub loads are intended as the rotor dynamic characteristics elements for use in the Simplified Coupled Rotor/Fuselage Vibration Analysis (SIMVIB).

Sections are included presenting updates to the development of the original G400 theory, and material appropriate to the user of the G400PA computer program. This material includes (1) a general description of the structuring of the G400PA FORTRAN coding, (2) a detailed description of the required input data and other useful information for successfully running the program, and (3) a detailed description of the output results.

* The research effort which led to the results in this report was financially supported by the Structures Laboratory, USARTL (AVRADCOM).

INTRODUCTION

The G400PA helicopter rotor aeroelastic analysis described herein represents a generalization and extension of the original United Technologies Research Center (UTRC) G400 Rotor Aeroelastic Analysis which was first described in Reference 1. This analysis was originally developed in response to the unique aeroelastic characteristics of the composite bearingless rotor and represented an advancement in the state-of-the-art with regard to the modeling of rotors with time-variable, nonlinear structural twist and multiple structural redundancy. Since the publication of Reference 1, the G400 analysis has evolved into a family of analyses with a completely general range of applicability in rotor type (articulated, hingeless, teetered) and vehicle application (helicopters, propellers, wind turbines).

The principal distinguishing features of the G400PA version of the analysis are:

1. A capability for analyzing underslung teetered rotors.
2. The implementation of the nonlinear equations of motion for two independent blade appended pendulum vibration absorbers.
3. Inclusion of the dynamic and aerodynamic loads due to specified harmonic accelerations in arbitrary combinations of all six components of hub motion.
4. The expansion of the blade pitch control description to include cosine and sine components of the $(b-1)$, b , and $(b+1)$ harmonics of cyclic pitch angle, (where b is the number of blades).
5. Provision for calculating impedance matrices, wherein each of the components of hub acceleration are systematically perturbed to obtain numerical partial derivatives of hub loads with respect to hub motion.

Since the original G400 analysis is well documented in Reference 1, this report presents only the technical background, and descriptions and/or formulations pertinent to the G400PA features listed above. Additional sections are presented to facilitate the user of the actual (G400PA) computer program. One section gives a general description of the structuring of the computer program with descriptions of all the program elements. Other sections give

complete descriptions of all required inputs for the program as well as descriptions of the output results. Although these input and output descriptions overlap to a large degree those given in Reference 1, they are presented for completeness. The appendix updates, where appropriate, the material of Reference 1.

LIST OF SYMBOLS

$[A]$	Inertia coupling matrix for a single blade.
$[AA]$	The combined inertia coupling matrix for the degrees-of-freedom of the two blades of a teetered rotor.
A_{n_s}, B_{n_s}	n 'th Fourier cosine and sine components, respectively, of inputted cyclic blade pitch control (higher harmonic control angles), deg.
$A_{qq}, A_{q\beta}, A_{\beta\beta}$	Submatrices comprising $[A]$.
b	Number of blades.
$c\psi, s\psi$	Abbreviated notation for cosine and sine of ψ , respectively.
C_p	Damper rate of explicit restraint of pendulum absorber about hinge, in-lb-sec/rad.
$DS1_i, DS2_i, DS3_k, DS4_k, DS5_j$	Integration constants used to calculate the blade internal loads immediately outboard of the flexbeam torque tube juncture, (ND).
e	x_2 coordinate of coincident flat-lag hinge or hingeless blade offset point, in.
f_i	Function defining fraction of pendulum absorber mass to be included in mass of i 'th blade segment, (ND).
$F_{x_5}, F_{y_5}, F_{z_5}$	Components of force in respective axis directions in the 5-coordinate system, lb.
h_{usl}	Distance rotor/blade apex point is below teeter hinge, in.
$[I_m]$	Identity matrix of dimension m .
I_p	Mass moment of inertia of pendulum absorber about its flapping hinge, in-lb-sec ² .
k_{y10}, k_{z10}	Mass radii of gyration of blade section about axes through and perpendicular to the spanwise (x_5) axis and in the chordwise and thicknesswise directions, respectively, in..

LIST OF SYMBOLS (Cont'd)

K_p	Spring rate of explicit restraint of pendulum absorber about hinge, ft-lb/rad.
K_{β_1}, K_{β_2}	Effective spring rates defining the nonlinear elastic characteristics of teeter stops, ft-lb/rad.
ℓ_p	Distance from hinge to mass center of a pendulum absorber, in.
m	Blade mass distribution, lb-sec ² /ft ² .
m_o	Reference blade mass distribution, defined by mass of the 5th blade segment, lb-sec ² /ft ² .
M_{PA}	Mass of pendulum absorber, lb-sec ² /ft.
$M_{x_5}, M_{y_5}, M_{z_5}$	Components of blade moment about axes in the 5- coordinate system, arising from inertia, aerodynamic and/or concentrated mechanical effects, ft-lb.
M_2	The saturation moment used in the nonlinear elastic characteristics of teeter stops, ft-lb.
n_I, n_O	Blade segment numbers of inner and outer segments bracketing pendulum absorber mass.
NEM, NFM, NTM	Numbers of assumed flatwise, edgewise, and torsion natural "uncoupled" primitive modes, respectively.
P_I	Differential operator denoting differentiation with respect to time of quantities measured in the inertial frame, sec ⁻¹ .
$P_{x_5}, P_{y_5}, P_{z_5}$	Section shear load distributions in directions of axes in the 5- coordinate system, lb/in.
q	General expression for a response variable deflection, (ND).
$\{q\}$	Vector of blade degrees-of-freedom excluding flapping motion.
q_{vk}	Blade k'th edgewise modal response variable, (ND).
q_{wi}	Blade i'th flatwise modal response variable, (ND).
$q_{x_5}, q_{y_5}, q_{z_5}$	Section moment load distributions about axes in the 5- coordinate system, in-lb/in.

LIST OF SYMBOLS (Cont'd)

$q_{\theta j}$	Blade j'th torsion modal response variable, (ND).
r	Blade spanwise coordinate, measured from offset, e , in x_5 direction, ft.
Δr_i	i'th blade spanwise segment length, ft.
R	Rotor radius, ft.
S_p	Amplitude of friction moment restraint of pendulum absorber about hinge, ft-lb.
$S_{x_5}, S_{y_5}, S_{z_5}$	Components of concentrated shear in directions of axes in the 5- coordinate system, lb.
t	Time, sec..
$[T_0], [T_1], [T_2], [T_5]$	Coordinate system transformation matrixes relating rotating coordinate system deflection to the inertial frame.
$\Delta v, \Delta w$	Deflection correction terms due to first order twist effects, (ND).
V_x, V_y, V_z	Components of instantaneous lineal velocity of the nonrotating hub in the hub fixed coordinate system, ft/sec.
$\{V_5\}$	Vector of components of velocity of a point in the coned, lead-lagged, rotating coordinate system, ft/sec.
$\Delta V, \Delta W$	Deflection correction terms due to second order twist effects, (ND).
x_5, y_5, z_5	Components of the 5- coordinate system, defined to be rotating with the hub, but at the blade coned and lagged position, ft.
$\{X_5\}$	Vector of components of displacement of a point in the coned, lead-lagged, rotating coordinate system.
y_{10}, z_{10}	Chordwise and thicknesswise position coordinate, respectively, of an arbitrary point within a blade section, in.
$y_{10_{CG}}$	Chordwise distance of blade section mass center from the reference axis, in.

LIST OF SYMBOLS (Cont'd)

z_4	Out of plane deflection in the unconed (and unflapped) coordinate system, ft.
$[Z]$	Higher harmonic impedance matrix (partial derivatives of hub loads with respect to hub acceleration and HHC angles).
β	Total cone angle, consisting of built-in and flapping (or teetering) contributions, rad.
β_B	Built-in blade precone, deg, rad. (as appropriate).
β_P	Flapping angle of blade appended pendulum vibration absorber, rad.
β_t	Teeter angle ($= \beta - \beta_P$), rad.
β_1, β_2	Angles defining the nonlinear elastic characteristics of teeter stops, deg.
γ_{v_k}	Deflection mode shape for the k'th edgewise normal mode, (ND).
γ_{w_i}	Deflection mode shape for the i'th flatwise normal mode, (ND).
γ_{θ_j}	Deflection mode shape for the j'th torsion normal mode, (ND).
δ	Blade lead angle, rad.
θ	Elastic torsion deflection angle, rad.
$\theta_{S_X}, \dots, \theta_{M_Z}$	Abbreviated torsion flexibility coefficients containing deflection dependency, rad/lb, rad/ft-lb.
θ_o	Blade pitch angle due to input control angle, rad.
$\theta_{o_{PAH}}$	Built-in inclination of pendulum absorber hinge axis relative to local chord line, deg, rad (as appropriate).
θ	Total local blade pitch angle, rad.
$\Delta\theta_J$	Total torsion deflection of flexbeam at junction point beyond built-in value, rad.
$\{E\}$	Vector of excitations for two-bladed teetering rotor degrees-of-freedom.

LIST OF SYMBOLS (Cont'd)

Ξ_q, Ξ_β	Component vectors of the Ξ excitation vector relating to modal excitations and flapping excitation, respectively.
$\Delta \Xi_{TS}$	The moment imparted to the teeter moment by the teeter stops.
ψ	Blade azimuthal (angular) position, rad.
$\omega_{w_i}, \omega_{v_k}, \omega_{\theta_j}$	(Nondimensional) uncoupled natural frequencies of i'th flatwise bending mode, k'th edgewise bending mode and j'th torsion mode, respectively, rad/sec.
$\omega_x, \omega_y, \omega_z$	Components of instantaneous rotational velocity of the non-rotating hub in the hub fixed coordinate system, rad/sec.
Ω	Rotor rotational frequency, rad/sec.

SUBSCRIPTS

$()_B$	Structurally built-in parameter, or conditions of blade immediately outboard of juncture.
$()_D$	Effect of dynamic origin.
$()_e$	Due to elastic deformation.
$()_h$	With respect to the nonrotating hub.
$()_{HHC}$	Higher harmonic blade pitch control
$()_I$	With respect to inertial space.
$()_J$	Conditions at flexbeam-torque tube juncture.
$()_P, ()_{PA}$	Pendulum absorber.
$()_{PAH}$	Pendulum absorber hinge.
$()_{TS}$	Pertaining to teeter stops.

LIST OF SYMBOLS (Cont'd)

SUPERSCRIPTS

- $()^{(m)}$ Pertaining to the m 'th blade of a teetered rotor
- $()^{\bar{}}$ Nondimensionalization by combinations of m_0, R and/or Ω .
- $()^*$ Differentiation with respect to (Ωt) .
- $()^r$ Differentiation with respect to (r/R) .

SIMULATION OF UNDERSLUNG TEETERED ROTORS

Basic Modeling Considerations

For articulated and hingeless rotor systems the individual rotor blades are mechanically coupled to each other only through motions of the hub. Consequently, these rotor types can be conveniently analyzed as single-bladed rotors whenever the assumption of infinite hub rigidity is involved. That is, without hub motion, the blades do not interact mechanically with each other. This is not true for teetered (two-bladed) rotors, however. Even for infinite impedance of the supporting shaft, each of the blades of a teetered rotor can impart bending loads to the other through the root load restraint. Accordingly, teetered rotors must be analyzed as a multiple (two) bladed rotor system.

The method of implementing the teetered rotor capability in the G400PA analysis was selected based upon the already inherent use of the Galerkin method of solution. The selected method actually amounts to a "modified Galerkin" approach in that the assumed uncoupled bending modes used to define the blade elastic deformations actually satisfy only the geometric boundary conditions. More specifically, the modeling is based upon the following considerations:

1. The rotor system is assumed to consist of a rigid body finite mass hub which teeters as a rigid body, and two blades which are each cantilever attached to this hub mass. Thus, the out-of-plane displacements for either blade consists of a rigid flapping part plus an elastic part based on "cantilevered" uncoupled mode shapes. For untwisted blades, this displacement distribution (for the n'th blade) assumes the following form (using the nomenclature of Reference 1):

$$z_4^{(m)}(r) = r \left[\beta_B + (-1)^{(m-1)} (\beta - \beta_B) \right] + \sum_{i=1}^{NEM} \gamma_{wi}(r) q_{wi}^{(m)}(t) \quad (m=1,2) \quad (1)$$

where $\gamma_{wi}(r)$ are the uncoupled cantilevered flatwise bending mode shapes. In this formulation, each of the $q_{wi}^{(m)}$ modal response quantities are independent degrees-of-freedom. The advantage of this formulation is that symmetric bending rotor modes, which respond typically at even harmonics, are simulated exactly, and the antisymmetric rotor modes, which respond typically at odd harmonics, can be well approximated geometrically as "pinned" modes with Equation (1).

2. The blade inplane deflections are simulated with no lead lag rotation, but with combinations of edgewise and flatwise bending as in a typical hingeless configuration.

3. The mass of the hub, to which the blades are cantilever attached, is set to zero as a limiting process. The required moment balance about the teeter hinge (in the flapping direction) is achieved by properly combining the flapping equations for the two blades together with the moment imparted to the teeter motion excitation by the teeter stops.

4. This formulation is inherently incapable of yielding correct bending moment calculations at the root region using mode deflection methods. This is because the formulation uses modes which do not satisfy the "load" boundary conditions at the root. Both the modified Galerkin formulation and the force-integration method, however, are relatively insensitive to these boundary conditions. Consequently, the bending moments and stresses obtained using force-integration, should be reasonably accurate.

The four considerations discussed above form the basis for the actual mathematical formulation discussed in the following subsections. In the first subsection, the load distributions resulting from the flapping motion of an underslung teetered blade are described. In the next subsection, the implementation of the moment equilibration across the teeter hinge is presented. Finally, in the last subsection, the details of the implementation of the teeter stop load characteristics are presented.

Aerodynamic and Dynamic Load Distributions

The analysis presented in Reference 1, and implemented in the parent G400 code, would be sufficient for formulating the teeter flap angle equation, but for the presence of the undersling distance, h_{usl} . This distance is defined as the distance of the rotor-hub apex below the teeter axis. The approach taken for defining the additional loads due to undersling is to define an incremental position vector and to then form the appropriate incremental components of inertial velocity and acceleration, as measured in the blade coordinate system. Using Equation (35) of Reference 1 as a starting point and referring to Figure 1, one can write the incremental (nondimensional) position vector as:

$$\Delta\{X_5\}_{usl} = h_{usl} \begin{Bmatrix} -\beta_B \\ 0 \\ -1 \end{Bmatrix} \quad (2)$$

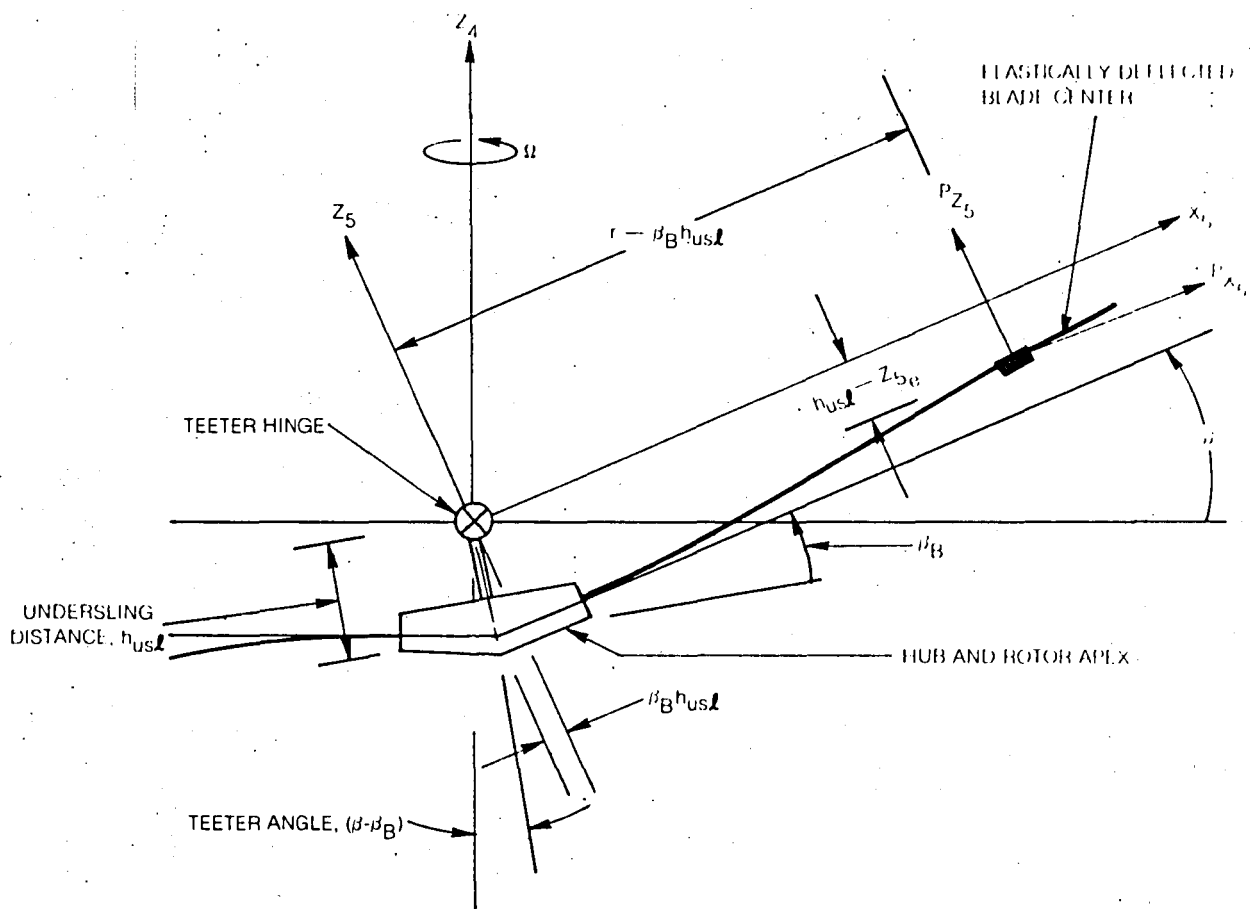


Figure 1. Schematic of Teetered Rotor System — Kinematic Definitions and Flapping Moment Equilibration

Using coordinate system transformations as described in Reference 1 and appropriate differentiation yields the following expression for incremental velocity vector:

$$\{\Delta v_5\}_{usl} = h_{usl} \begin{Bmatrix} \dot{\beta}^* \\ \beta - \beta_B \\ 0 \end{Bmatrix} \quad (3)$$

This vector then modifies the definition for blade section inflow angle used for defining the quasi-static angle-of-attack, and finally the blade air-load distribution. Further use of the coordinate system transformations, additional differentiation and D'Alembert's principle, yields the following vector for the incremental (inertial) dynamic load distribution:

$$\Delta \begin{Bmatrix} p_{Dy5} \\ p_{Dy5} \\ p_{Dy5} \end{Bmatrix} = -\overline{m} h_{usl} \begin{Bmatrix} \beta^{**} - (\beta - \beta_B) \\ 2 \dot{\beta}^* \\ -\beta [\beta^{**} - (\beta - \beta_B)] \end{Bmatrix} \quad (4)$$

Before the teetered blade root constraint can be implemented, the basic flapping equation must also be modified to account for the undersling distance. With reference to Figure 1, equilibration of the moment about the flapping hinge results in the following modified flapping equation:

$$\int_0^1 [(r - h_{usl} \beta_B) p_{z5} - (z_{5e} - h_{usl}) p_{x5} - q_{y5}] dr - M_{y5} = 0 \quad (5)$$

This modified equation is to be compared with Equation (31) of Reference 1. Note that p_{x5} and p_{z5} are, respectively, the total load distributions in the x_5 - and z_5 - directions and contain the incremental loads given by Equation (4). The loads due to teeter stops are accounted for by the general moment about the flapping hinge, M_{y5} , this moment defined in greater detail in the following subsection.

Implementation of Teetered Blade Root Constraint

As implemented by the G400 analysis for a single blade (infinite impedance hub), the blade equations of motion take the following form:

$$\begin{bmatrix} A_{qq} & A_{q\beta} \\ A_{q\beta} & A_{\beta\beta} \end{bmatrix} \begin{Bmatrix} \ddot{q}^* \\ \ddot{\beta}^* \end{Bmatrix} = \begin{Bmatrix} \Xi_q(\psi) \\ \Xi_\beta(\psi) \end{Bmatrix} \quad (6)$$

In this form, the elastic mode acceleration subvector, $\{\ddot{q}^{**}\}$, and the flapping acceleration, $\ddot{\beta}$, are linearly coupled, and all remaining linear and nonlinear terms in the various equations are grouped on the right-hand side as an excitation vector. This vector is composed of a subvector for the elastic modes, $\{\Xi_q\}$, and the term for the flapping equations, $\{\Xi_\beta\}$. This form of the equations is appropriate for time-history solutions, but requires a simultaneous equations solution at each time step to decouple the accelerations.

Before two blades are mechanically constrained by the teetered blade boundary conditions, Equation (6) must be generalized to the following augmented form:

$$\begin{bmatrix} A_{qq}^{(1)} & A_{q\beta}^{(1)} & 0 \\ A_{q\beta}^{(1)T} & A_{\beta\beta} & 0 \\ 0 & 0 & A_{qq}^{(2)} & A_{q\beta}^{(2)} \\ 0 & 0 & A_{q\beta}^{(2)T} & A_{\beta\beta} \end{bmatrix} \begin{Bmatrix} \ddot{q}^{*(1)} \\ \ddot{\beta}^{*(1)} \\ \ddot{q}^{*(2)} \\ \ddot{\beta}^{*(2)} \end{Bmatrix} = \begin{Bmatrix} \Xi_q^{(1)} \\ \Xi_\beta^{(1)} \\ \Xi_q^{(2)} \\ \Xi_\beta^{(2)} \end{Bmatrix} \quad (7a)$$

or, in a more abbreviated form as:

$$[AA]\{\ddot{Q}^{**}\} = \{\Xi\} \quad (7b)$$

The teetered constraint can be conveniently implemented by first defining the following constraint relationship:

$$\{\ddot{Q}^{**}\} = \begin{bmatrix} 1 & 0 & 0 & 0 \\ 0 & 1 & 0 & 0 \\ 0 & 0 & 1 & 0 \\ 0 & 0 & 0 & 1 \end{bmatrix} \begin{Bmatrix} \ddot{q}^{*(1)} \\ \ddot{\beta}^{*(1)} \\ \ddot{q}^{*(2)} \\ \ddot{\beta}^{*(2)} \end{Bmatrix} \quad (8a)$$

$$= [\tilde{T}]\{\ddot{\tilde{Q}}^{**}\} \quad (8b)$$

The teeter constraint is applied to the equations of motion, Equation (7), with the following matrix operations:

$$[T^T][AA][T]\begin{Bmatrix} \ddot{Q} \end{Bmatrix} = [T^T]\{\Xi\} + \{\Delta\Xi\}_{TS} \quad (9)$$

The partitioning of Equation (9) is as follows:

$$\begin{bmatrix} A_{qq}^{(1)} & A_{q\beta}^{(1)} & 0 \\ A_{q\beta}^{(1)T} & 2A_{\beta\beta} & -A_{q\beta}^{(2)T} \\ 0 & -A_{q\beta}^{(2)} & A_{qq}^{(2)} \end{bmatrix} \begin{Bmatrix} \ddot{q}^{(1)} \\ \ddot{\beta}^{(1)} \\ \ddot{q}^{(2)} \end{Bmatrix} = \begin{Bmatrix} \Xi_q^{(1)} \\ \Xi_\beta^{(1)} - \Xi_\beta^{(2)} + \Delta\Xi_{TS} \\ \Xi_q^{(2)} \end{Bmatrix} \quad (10)$$

Equation (10) is then in the same form as Equation (6) and the same procedure must be followed to achieve a time-history solution (decoupling of the accelerations and then numerical integration). Generally, the simultaneous equations solution of Equation (10) is accomplished using partitioning methods; the details of this essentially mathematical operation are outside the scope of this report and are therefore omitted.

Teeter Stop Moment Characteristics

The moment applied to the teeter angle equation due to the teeter stops, $\Delta\Xi_{TS}$, is an essentially nonlinear function of teeter angle. This moment is characterized in the G400PA analysis by the five parameters defined graphically in Figure 2. For teeter angles between $\pm \beta_1$, the teeter stop moment is, of course, zero. When the teeter angle reaches the first limit stop angle, β_1 , the limit stop imparts an initially elastic reaction with a spring rate of K_{β_1} . Between this first limit stop angle and a saturation angle, β_2 , the reaction moment is assumed to be a generally nonlinear function of teeter angle and increases to the value of M_2 with a rate of K_{β_2} , at the saturation angle, β_2 . At teeter angles above β_2 , the reaction moment again obeys an elastic relationship. Generally, the saturation spring rate, K_{β_2} , will exceed the initial rate, K_{β_1} . However, this implementation provides sufficient latitude for modeling other nonlinear relationships. Mathematically, this implementation can be defined as follows:

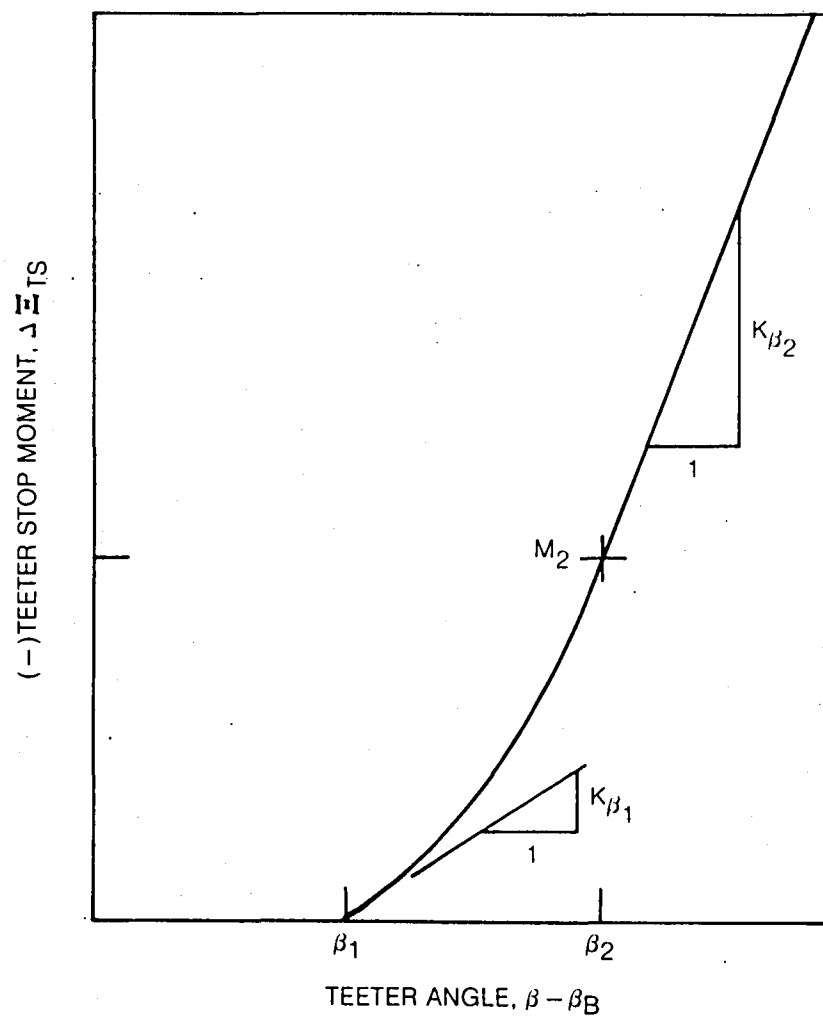


Figure 2. Generalization of Nonlinear Teeter Stop Moment vs Teeter Angle Characteristics

$$\begin{aligned}
& 0, |\beta_1| \leq \beta_1 \\
& -\operatorname{sgn} \beta \left\{ K_{\beta_1} \frac{(|\beta_1| - \beta_1)(|\beta_1| - \beta_2)^2}{\Delta \beta_{12}^2} \right. \\
& \left. + M_2 \left[1 - \frac{2(|\beta_1| - \beta_2)}{\Delta \beta_{12}} \right] \left(\frac{|\beta_1| - \beta_1}{\Delta \beta_{12}} \right)^2 \right. \\
& \left. + K_{\beta_2} \frac{(|\beta_1| - \beta_2)}{\Delta \beta_{12}^2} (|\beta_1| - \beta_1)^2 \right\}, \beta_1 \leq |\beta_1| \leq \beta_2 \\
& -\operatorname{sgn} \beta [K_{\beta_2} (|\beta_1| - \beta_2) + M_2], \beta_2 \leq |\beta_1| < \infty
\end{aligned} \tag{11}$$

BLADE APPENDED PENDULUM VIBRATION ABSORBERS

Basic Assumptions

The inclusion of blade appended pendulum absorbers in the aeromechanical description of the rotor blade requires the definition of additional equations of motion, as well as modifications to existing ones. The following list of principal assumptions forms the basis of the G400PA modeling of blade appended pendulum absorbers:

1. Provision must be made for simulating a maximum of two (2) independent pendular absorbers. State-of-the-art installations of such vibration absorbers have included up to two absorbers, each tuned to a different rotor harmonic.

2. Each pendular absorber consists of a specified hinge location, a rigid body mass (with c.g. offset and rotary inertia about that hinge), and a restraint about the hinge accruing from a rotary spring, a rotary viscous damper, and a (nonlinear) friction damper (see Figure 3).

3. The hinge location and orientation for each absorber is subject to the following constraints (again refer to Figure 3):

a. The hinge axis must be within a blade section plane, e.g., perpendicular to the spanwise axis.

b. The hinge axis may be both translated and inclined relative to the local chord line. This translation and inclination define the distance, z_{10PAH} , and the angle, θ_{0PA} , shown in Figure 3.

c. The hinge axis may be located at any spanwise station.

4. The mass center of each absorber is nominally chordwise balanced at the blade elastic (reference) axis, (i.e., no chordwise mass offset, $y_{10PA} = 0$) in the undeflected position. Note that for nonzero values of inclination angle (of the hinge axis relative to the chord line), deflections of the pendulum will produce time variable chordwise c.g., offsets.

5. To enable the analysis to make rapid parameter variations on the pendular parameters, the blade bending and torsion modes are calculated excluding the mass of the pendula. Therefore, the effect of incremental pendulum mass must be explicitly accounted for in the blade dynamic equations. This is accomplished by adding the respective pendulum masses as incremental mass distributions extended over the two blade segments which straddle that pendulum's radial location.

6. Lastly, the pendula deflection angles are not restricted to "small" amplitudes. Thus, the realistic effects of amplitude saturation can be analyzed.

Dynamic Loads

The derivation of the dynamic loads acting on the pendulum follows the basic method described in the previous chapter wherein an incremental displacement vector is defined, and then with appropriate differentiation and coordinate transformations an inertial acceleration vector is formed. The displacement vector for a point mass hinged to an offset, inclined axis is given by:

$$\Delta \{X_5\}_{PA} = l \begin{Bmatrix} \cos \beta_p \\ -\sin \Theta_{PAH} \sin \beta_p \\ \cos \Theta_{PAH} \sin \beta_p \end{Bmatrix} + Z_{IO_{PAH}} \begin{Bmatrix} 0 \\ -\sin \Theta \\ \cos \Theta \end{Bmatrix} \quad (12)$$

where the total pitch angle of the hinge axis, Θ_{PAH} , is the sum of the blade pitch axis, Θ , and the built-in pitch angle relative to the blade, Θ_{OPA} . The resulting components of inertia loading are then given by the following equations:

$$\begin{aligned} (\Delta p_{DX_5})_{PA} = \frac{-M_{PA} f_i l}{m_0 \Delta r_i} & \left[-\sin \beta_p \ddot{\beta}_p^* - \cos \beta_p + 2 \cos \beta_p \ddot{\beta}_p^* \sin \Theta_{PAH} \right. \\ & \left. + (\beta + 2\ddot{\Theta}) \sin \beta_p \cos \Theta_{PAH} \right] \end{aligned} \quad (13a)$$

$$\begin{aligned} (\Delta p_{DY_5})_{PA} = \frac{-M_{PA} f_i}{m_0 \Delta r_i} & \left\{ l \left[-\cos \beta_p \sin \Theta_{PAH} \ddot{\beta}_p^* - 2 \sin \beta_p \ddot{\beta}_p^* \right. \right. \\ & \left. + \sin \beta_p (1 + 2\ddot{\delta} + \ddot{\beta}_p^{*2} + \ddot{\Theta}^2) \sin \Theta_{PAH} \right. \\ & \left. - (2 \cos \beta_p (\ddot{\beta}_p^* \ddot{\Theta} + \beta \ddot{\beta}_p^*) + \sin \beta_p (2\beta + \ddot{\Theta})) \cos \Theta_{PAH} \right] \\ & + Z_{IO_{PAH}} \left[-2 (\ddot{w}_e^* - \Delta \ddot{w}^{(2)} - \Delta \ddot{w}^{(2)}) - (\ddot{\Theta} + 2\ddot{\beta}) \cos \Theta \right. \\ & \left. + (1 + \ddot{\Theta} + 2\beta \ddot{\Theta} + 2\ddot{\delta}) \sin \Theta \right] \left. \right\} \end{aligned} \quad (13b)$$

$$\begin{aligned}
\left(\Delta p_{DZ_5}\right)_{PA} = & \frac{-M_{PA} f_i}{m_0 \Delta r_i} \left\{ l \left[\cos \beta_p \cos \Theta_{PAH} \ddot{\beta}_p \right. \right. \\
& - (2 \cos \beta_p (\dot{\beta}_p^* \dot{\theta} + \beta_p^* \ddot{\theta}) + \sin \beta_p^* \ddot{\theta}) \sin \Theta_{PAH} - \sin \beta_p (\dot{\beta}^2 + \dot{\theta}^2 + 2 \beta \dot{\theta}) \cos \Theta_{PAH} \left. \right] \\
& + Z_{IO_{PAH}} \left[-(\dot{\Theta}^2 + 2 \beta \dot{\Theta} + \beta^2) \cos \Theta - \dot{\Theta}^* \sin \Theta \right] \left. \right\} \quad (13c)
\end{aligned}$$

where the distribution function, f_i , is defined for only two of the blade spanwise segments, the centers form a straddling pair: the one closest in-board, $r(n_I)$, and the one closest outboard, $r(n_O)$, of the pendulum mass center location, r_{PA} : (see Figure 4):

$$f_i = \begin{cases} \frac{r(n_O) - r_{PA}}{r(n_O) - r(n_I)} & ; i = n_I \\ \frac{r_{PA} - r(n_I)}{r(n_O) - r(n_I)} & ; i = n_O \end{cases} \quad (14)$$

Equations (13) and (14) are then in a general form appropriate for inclusion in the blade dynamic equations. Note that the nominal inertia load distributions, given by Equations (41a, b, c) and (44a, b, c) of Reference 1 must also be modified since, at the two straddling radial stations, the mass distributions must be augmented by $M_{PA} f_i$.

Equations of Motion

The usual blade dynamic equations (those for modal responses, flapping and lead-lag motions) are easily modified by including the additional inertia load distributions as defined in the above subsection. The pendulum equations are formed by equilibrating the inertia moments about the hinge to the spring and damper restraints:

$$I_p \ddot{\beta}_p^* = l \left[\cos \beta_p F_{Z_6} - \sin \beta_p F_{X_5} \right] - K_p \beta_p - C_p \dot{\beta}_p - S_p \operatorname{sgn}(\dot{\beta}_p) \quad (15)$$

where the concentrated loads acting on a pendulum mass center, F_{X_5} and F_{Z_6} , are given by:

$$F_{X_5} = \tilde{p}_{X_5} + \Delta \tilde{p}_{X_5} \quad (16a)$$

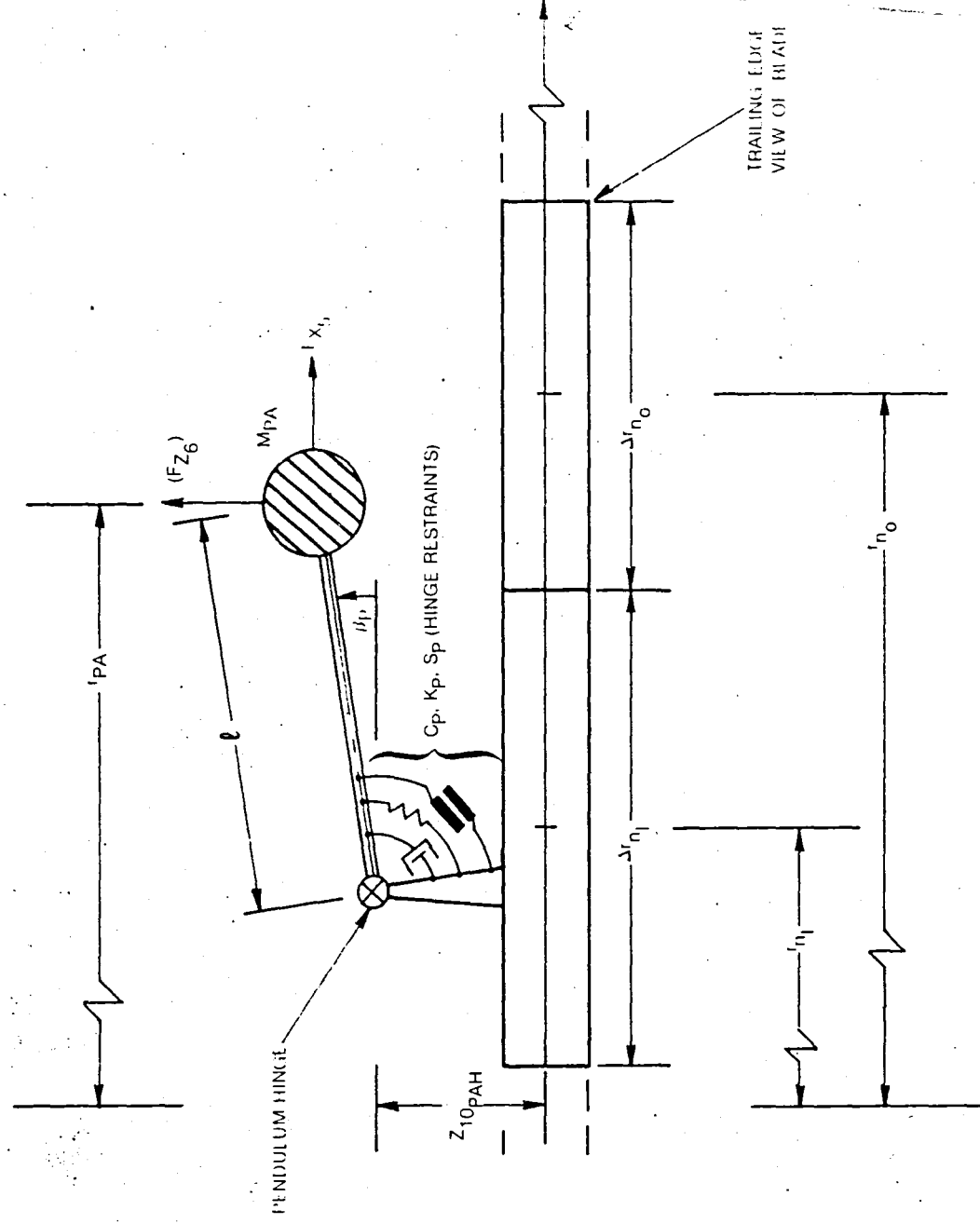


Figure 4. Blade Trailing Edge View of Blade/Pendular Absorber System — Kinematic Definitions and Moment Equilibration

$$F_{z_6} = -\sin \theta_{PAH} (\tilde{p}_{y_5} + \Delta \tilde{p}_{y_5}) + \cos \theta_{PAH} (\tilde{p}_{z_5} + \Delta \tilde{p}_{z_5}) \quad (16b)$$

and where the quantities \tilde{p}_{x_5} , \tilde{p}_{y_5} , \tilde{p}_{z_5} are components of the usual blade inertia loadings for the straddling segments modified by the following multiplication:

$$\tilde{p}_{PA} = \sum_{i=n_1}^{n_0} \frac{M_{PA} f_i}{m_0 \Delta r_i \bar{m}} p(r_i) \quad (17)$$

The quantities, $(\Delta \tilde{p}_{x_5}$, $\Delta \tilde{p}_{y_5}$ and $\Delta \tilde{p}_{z_5}$ are formed from Equations (13a, b and c), respectively, but with the factor $(f_i / m_0 \Delta r_i)$ set equal to unity, and all the β^{**} dependent terms deleted. All such β^p terms are instead grouped into the single inertia-acceleration term on the left-hand side of Equation (15). Note that I_p is the effective rotary inertia of the pendulum about the hinge. The above development is the same for either pendulum and subscripting to denote pendulum index was omitted for clarity.

BLADE LOADS DUE TO HIGHER HARMONIC EXCITATIONS

As originally formulated, the G400 aeroelastic analysis simulated a wide spectrum of "higher harmonic" blade loads. The term "higher harmonic" is used herein to denote frequency content in the range of blade number (b) x rotor rotation frequency (Ω), and above. Indeed, because of the multi-harmonic nature of the local dynamic pressure of helicopter blade section in forward flight, higher harmonic airloads ensue even from the usual collective and simple harmonic cyclic blade pitch angles. Another explicit source of higher harmonic airloads is the considerable harmonic variability of the inflow velocities induced in the rotor plane by the vortex structure of the rotor itself. Reference (2) presents an in-depth description of this theory and its interactive implementation with the G400 analyses.

Two further sources of higher harmonic excitation are considered herein. The first, prescribed harmonic motion of the hub, is required to evaluate the characteristics of the rotor coupling with the airframe. This coupling is accomplished in the Simplified Coupled Rotor/Airframe Vibration Analysis (SIMVIB) using the rotor impedance matrices computed in the G400PA code. The details of this calculation are described in a subsection below. The second source of higher harmonic excitation considered, higher harmonic pitch control, is included to provide an important analytic capability for application to a timely area of helicopter vibration of research and development. Technical developments of each of these sources of higher harmonic excitation are presented in the subsections which follow.

Prescribed Harmonic Hub Motions

The required impedance matrix is the collection of partial derivatives of the six components of hub vibratory loads (3 shears and 3 moments) with respect to each of the six components of hub vibratory acceleration (3 translations and 3 rotations). This calculation is generally implemented by first achieving harmonic responses with selective perturbations in each of the components of acceleration and then forming numerical partial derivatives of the hub loads. The actual hub loads are calculated using the force-integration method (see Reference 3) together with the total resulting inertia, gravity and aerodynamic blade load distributions. The details of this calculation do not represent new technology and, consequently, are omitted herein.

Of more importance are the calculations of the incremental airloads and dynamic loads due to harmonic hub motion. For this purpose, the components of inertia velocity and acceleration, in the blade coordinate system are required. Generally, the hub degrees-of-freedom are defined in the non-rotating (with rotor speed, Ω) body-fixed axis system; therefore, the basic degrees-of-freedom are the instantaneous velocity components along (or about) coordinate axes fixed to the "nonrotating", but generally moving hub. Because of this definition of basic hub degrees-of-freedom, the actual deflections (translations and rotations) are subject to the order of integration and the appropriate Euler angles must be suitably defined and integrated in this context. Furthermore, recourse must be made to the Theorem of Coriolis (Reference 4) to obtain the correct differentiation with respect to time as measured in an inertial space. The material to follow outlines the approach for making these differentiations and obtaining their components in the blade coordinate system. Much intermediate calculation is omitted for clarity, and the final results include the previously considered effects of undersling (teetered rotor feature) and thickness noise mass center off-sets (pendulum absorber feature).

Consider the vector sum for a point mass at a blade section:

$$\vec{X}_I = \vec{X}_O + \vec{X}_1 + \vec{X}_2 \quad (18)$$

where X_I is the position vector with respect to inertial space. X_O is the position vector of the nonrotating (with respect to Ω) hub:

$$\{X_O\} = [T_O] \{X_h\} \quad (19)$$

$[T_O]$ is the coordinate transformation due to hub orientation motion and $\{X_h\}$ is the position vector of the hub in the hub fixed system. Consistent with the definition of the hub centered coordinate system, $[T_O]$ and $\{X_h\}$ can be considered to be unity and null, respectively, at any instant in time, but have finite time derivatives. $\{X_1\}$ is the position vector of the offset/blade root point:

$$\{X_1\} = [T_O][T_1]\{e\} \quad (20)$$

where $[T_1]$ is the coordinate system transformation due to rotor rotation, and $\{e\}$ is the position vector from the hub center to the blade root point. $\{X_2\}$ is the position vector due to blade element displacement within the blade coordinate system:

$$\{X_2\} = [T_O][T_1][T_2]\{X_s\} \quad (21)$$

where $[T_2]$ is the coordinate transformation due to flapping and lead-lag about a common point, and $\{X_5\}$ is the position vector of the point mass within the blade "5" coordinate system. Specific definitions for the coordinate transformations and position vectors are as follows:

$$[T_0] = \begin{bmatrix} 0 & -\omega_z & \omega_y \\ \omega_z & 0 & -\omega_x \\ -\omega_y & \omega_x & 0 \end{bmatrix} \quad (22a)$$

$$[T_1] = \begin{bmatrix} c\psi & -s\psi & 0 \\ s\psi & c\psi & 0 \\ 0 & 0 & 1 \end{bmatrix} \quad (22b)$$

$$[T_2] = \begin{bmatrix} 1 & -\delta & -\beta \\ \delta & 1 & 0 \\ \beta & 0 & 1 \end{bmatrix} \quad (22c)$$

$$\{e\} = \begin{Bmatrix} \bar{e} + \bar{h}_{usl}(\beta - \beta_B) \\ 0 \\ -\bar{h}_{usl} \end{Bmatrix} \quad (22d)$$

$$\{X_5\} = \begin{Bmatrix} \bar{r} + \epsilon_x \\ \bar{y}_{10} c\Theta - \bar{z}_{10} s\Theta + \epsilon_y \\ \bar{y}_{10} s\Theta + \bar{z}_{10} c\Theta + \epsilon_z \end{Bmatrix} \quad (22e)$$

where ϵ_x , ϵ_y and ϵ_z are the elastic deflections in the x_5 , y_5 and z_5 directions, respectively, and \bar{r} , \bar{y}_{10} and \bar{z}_{10} are functions of the modal responses, structured twist, etc. Furthermore, for convenience, a matrix $[T_5]$ is defined which transforms from the nonrotating blade root to the blade "5" coordinate system:

$$[T_5] = [T_1][T_2] \quad (23)$$

Other operations on the T_5 matrix which are useful:

$$[T_5]^{-1} = \begin{bmatrix} 1 & \delta & \beta \\ -\delta & 1 & 0 \\ -\beta & 0 & 1 \end{bmatrix} \begin{bmatrix} c\psi & s\psi & 0 \\ -s\psi & c\psi & 0 \\ 0 & 0 & 1 \end{bmatrix} \quad (24)$$

$$[T_5^*] = \begin{bmatrix} -[(1+\delta^*)s\psi + \delta c\psi] & -[(1+\delta^*)c\psi + \delta s\psi] & [\beta s\psi - \beta^* c\psi] \\ [(1+\delta^*)c\psi - \delta s\psi] & -[(1+\delta^*)s\psi + \delta c\psi] & -[\beta c\psi + \beta^* s\psi] \\ \beta^* & 0 & 0 \end{bmatrix} \quad (25)$$

The total inertial velocity vector, is defined using the Theorem of Coriolis and is given in matrix form as follows:

$$\begin{aligned} p_I \{X_I\} = & [T_0] \{\dot{X}_h\} + \left[[T_0][T_1] + [T_0][T_1] \right] \{e\} \\ & + [T_0][T_1] \{\ddot{e}\} + \left[[T_0][T_5] + [T_0][T_5] \right] \{X_5\} + [T_0][T_5] \{\dot{X}_5\}. \end{aligned} \quad (26)$$

where the operator p_I denotes differentiation with respect to time, as measured in the inertial coordinate frame.

The terms underlined are deleted because they do not contribute to hub motion. Note that in this formulation, the actual hub deflections (translations and rotations) are taken as zero at any instant in time.

Transformation into components in the "5" coordinate system is accomplished by premultiplication by $[T_5]^{-1}$, and retention of only those terms relating to hub motion and/or undersling results in the following:

$$\begin{aligned} \{\Delta V_5\} = & [T_5]^{-1} \{\dot{X}_5\} \\ = & \begin{Bmatrix} v_x(c\psi - \delta s\psi) + v_y(s\psi + \delta c\psi) + \beta v_z \\ -v_x(s\psi + \delta c\psi) + v_y(c\psi - \delta s\psi) \\ -\beta(v_x c\psi + v_y s\psi) + v_z \end{Bmatrix} + \bar{e} \begin{Bmatrix} \omega_z \delta \\ \omega_z \\ -\omega_y c\psi + \omega_x s\psi \end{Bmatrix} \\ & + \bar{h}_{usl} \begin{Bmatrix} \omega_x s\psi - \omega_y c\psi \\ \omega_y s\psi + \omega_x c\psi + (\beta - \beta_B)\omega_z \\ 0 \end{Bmatrix} + \bar{r} \begin{Bmatrix} 0 \\ \omega_z - \beta(\omega_y s\psi + \omega_x c\psi) \\ -\omega_y(c\psi - \delta s\psi) + \omega_x(s\psi + \delta c\psi) \end{Bmatrix} \\ & - (\bar{y}_{10} c\Theta - \bar{z}_{10} s\Theta) \begin{Bmatrix} -\omega_z + \beta(\omega_x c\psi + \omega_y s\psi) \\ 0 \\ \omega_x c\psi + \omega_y s\psi \end{Bmatrix} + (\bar{y}_{10} s\Theta + \bar{z}_{10} c\Theta) \begin{Bmatrix} \omega_y c\psi - \omega_x s\psi \\ -(\omega_y s\psi + \omega_x c\psi) \\ 0 \end{Bmatrix} \end{aligned} \quad (27)$$

Equation (27) then gives the components of incremental velocity at the local blade section with which the tangential and normal components of air velocity, U_T and U_N , respectively, can be appropriately modified. The total blade section in flow angle, $\phi (= \tan^{-1} (U_N/U_T))$, is then formed in the usual manner and included in the section angle-of-attack. In this manner, the effects of prescribed hub motion are included in the airload distribution.

The inertia (dynamic) load distributions require the second time derivative with respect to inertial space. The Theorem of Coriolis is now applied to the velocity vector, Equation (26), rather than the displacement vector:

$$\begin{aligned}
 \rho_I \{ \rho_I \dot{X}_I \} = & [T_0] \{ \ddot{X}_h \} + [\dot{T}_0] \{ \dot{X}_h \} \\
 & + 2 \left[\begin{aligned} & [\dot{T}_0][T_1] + \underline{[T_0][\dot{T}_1]} \end{aligned} \right] \{ \dot{e} \} + \underline{[T_0][T_5]} \{ \ddot{X}_5 \} \\
 & + \left[\begin{aligned} & [\dot{T}_0^*][T_1] + 2 [\dot{T}_0][\dot{T}_1] + \underline{[T_0][\dot{T}_1^*]} \end{aligned} \right] \{ e \} + \underline{[T_0][T_1]} \{ \dot{e} \} \\
 & + 2 \left[\begin{aligned} & [\dot{T}_0][T_5] + \underline{[T_0][\dot{T}_5]} \end{aligned} \right] \{ \dot{X}_5 \} \\
 & + \left[\begin{aligned} & [\dot{T}_0^*][T_5] + 2 [\dot{T}_0][\dot{T}_5] + \underline{[T_0][\dot{T}_5^*]} \end{aligned} \right] \{ X_5 \}
 \end{aligned} \tag{28}$$

The underlined terms are deleted because they do not contain contributions accruing from hub motion. After the indicated operations have been performed, the following expressions for incremental components of inertia load distribution are obtained:

$$\begin{aligned}
\Delta \begin{Bmatrix} p_{Dx5} \\ p_{Dy5} \\ p_{Dz5} \end{Bmatrix} = & -\bar{m} \left\{ \begin{aligned} & \beta(\dot{V}_z - \omega_y V_x + \omega_x V_y) + (\dot{V}_x - \omega_z V_y + \omega_y V_z) c(\psi + \delta) + (\dot{V}_y + \omega_z V_x - \omega_x V_z) s(\psi + \delta) \\ & (\dot{V}_y + \omega_z V_x - \omega_x V_z) c(\psi + \delta) - (\dot{V}_x - \omega_z V_y + \omega_y V_z) s(\psi + \delta) \\ & \dot{V}_z - \omega_y V_x + \omega_x V_y - \beta[(\dot{V}_x - \omega_z V_y + \omega_y V_z) c\psi + (\dot{V}_y + \omega_z V_x - \omega_x V_z) s\psi] \end{aligned} \right\} \\
& + (\bar{r} + \bar{e}) \left\{ \begin{aligned} & -2[\omega_x - \beta(\omega_x c\psi + \omega_y s\psi)] \\ & \dot{\omega}_z - \beta(\dot{\omega}_x c\psi + \dot{\omega}_y s\psi) \\ & 2\beta\omega_z - (\dot{\omega}_y - 2\omega_x) c(\psi + \delta) + (\dot{\omega}_x + 2\omega_y) s(\psi + \delta) \end{aligned} \right\} \\
& + \bar{e} \left\{ \begin{aligned} & \dot{\omega}_z \delta - \beta(\dot{\omega}_y c\psi - \dot{\omega}_x s\psi) \\ & 2\omega_z \delta + \beta(\dot{\omega}_x c\psi + \dot{\omega}_y s\psi) \\ & -\delta[(\dot{\omega}_x + 2\omega_y) c\psi + (\dot{\omega}_y - 2\omega_x) s\psi] \end{aligned} \right\} \\
& + (\bar{y}_{10} c\Theta) - \bar{z}_{10} s\Theta \left\{ \begin{aligned} & -\dot{\omega}_z + [\beta\dot{\omega}_x + 2(\beta + \dot{\theta}_0)\omega_y] c\psi + [\beta\dot{\omega}_y - 2(\beta + \dot{\theta}_0)\omega_x] s\psi \\ & 2[-\omega_z - \dot{\theta}_0(\omega_x c\psi + \omega_y s\psi)] \\ & \beta\dot{\omega}_z + (\dot{\omega}_x + 2\omega_y) c\psi + (\dot{\omega}_y - 2\omega_x) s\psi \end{aligned} \right\} \quad (29) \\
& + \bar{h}_{usl} \left\{ \begin{aligned} & \dot{\omega}_x s\psi - \dot{\omega}_y c\psi - 2(\beta - \beta_B)\omega_z \\ & (\beta - \beta_B)\dot{\omega}_z + \dot{\omega}_x c\psi + \dot{\omega}_y s\psi \\ & \beta_B(\dot{\omega}_y c\psi - \dot{\omega}_x s\psi) + 2(\beta - \beta_B)(\omega_y s\psi + \omega_x c\psi) \end{aligned} \right\} \\
& + (\bar{y}_{10} s\Theta + \bar{z}_{10} c\Theta) \left\{ \begin{aligned} & 2(\beta + \theta_0)\omega_z + \dot{\omega}_y c(\psi + \delta) - \dot{\omega}_x s(\psi + \delta) \\ & -\beta\dot{\omega}_z - \omega_x c(\psi + \delta) - \dot{\omega}_y s(\psi + \delta) \\ & -2(\beta + \theta_0)(\omega_x c\psi + \omega_y s\psi) \end{aligned} \right\} \Bigg\rangle
\end{aligned}$$

In both Equations (27) and (28) the expressions for hub velocity and acceleration are completely general. For present purposes, these components of velocity and acceleration are to be prescribed as simple (but higher) harmonic functions:

$$\begin{Bmatrix} v_j \\ \omega_j \end{Bmatrix} = \begin{Bmatrix} v_{jnc} \\ \omega_{jnc} \end{Bmatrix} c(n\psi) + \begin{Bmatrix} v_{jns} \\ \omega_{jns} \end{Bmatrix} s(n\psi) \quad (30)$$

where $j = x, y, \text{ or } z$, and where n is equal to a prescribed multiple of the number of blades. To minimize the computational requirements for calculating these trigonometric functions, the following identities are utilized:

$\frac{n}{1}$	$\frac{c(n\psi)}{c\psi}$	$\frac{s(n\psi)}{s\psi}$	
2	$1 - 2(s\psi)^2$	$2(s\psi)(c\psi)$	
3	$4(c\psi)^3 - 3(c\psi)$	$3(s\psi) - 4(s\psi)^3$	(31)
≥ 4	$2c(n-1)\psi c\psi - c(n-2)\psi$	$2s(n-1)\psi c\psi - s(n-2)\psi$	

Higher Harmonic Blade Pitch Control

The implementation of higher harmonic pitch control (HHC) in the G400PA analysis is a relatively straightforward task. For this type of higher harmonic excitation, the incremental blade pitch angle is assumed to be of the following form:

$$\begin{aligned} \Delta\theta_{HHC} = & -A_{n-1s} c(b-1)\psi - B_{n-1s} s(b-1)\psi \\ & -A_{ns} c(b\psi) - B_{ns} s(b\psi) \\ & -A_{n+1s} c(b+1)\psi - B_{n+1s} s(b+1)\psi \end{aligned} \quad (32)$$

The amplitudes in this partial Fourier series are generally prescribed, or are perturbed in order to obtain the partial derivative matrix of hub loads with respect to HHC pitch amplitudes. The incremental pitch control angle given by Equation (32) is then used to define the blade airloads and to complete the calculations for θ_o , θ_o^* and θ_o^{**} used in forming the blade inertia load distributions.

Impedance Matrix Calculation

The impedance matrix is defined as the array of partial derivatives of components of hub loads with respect to components of higher harmonic excitation variables.

$$[Z] = \begin{bmatrix} \frac{\partial(X_{c_i}, X_{s_i})}{\partial(q_{c_j}, q_{s_j})} \end{bmatrix} \quad \begin{matrix} 1 \leq i \leq 6 \\ 1 \leq j \leq 9 \end{matrix} \quad (33)$$

These X_{c_i} and X_{s_i} terms are, respectively, the cosine and sine components of each of the six components of hub load, X_I , and similarly q_{c_j} and q_{s_j} are, respectively, the cosine and sine components of the higher harmonic excitation variables, q_j . Specifically, these consist of each of the six components of hub vibratory amplitude (cosine and sine) and three higher harmonic control pitch amplitudes (cosine and sine). The calculations for these derivatives are accomplished numerically by first obtaining responses which are converged to periodicity without, and then, with perturbations in each of the higher harmonic excitation variables, q_j :

$$\frac{\partial X_i}{\partial q_j} \approx \frac{X_i(q_j + \Delta q_j) - X_i(q_j)}{\Delta q_j} \quad (34)$$

In practice, the perturbation amplitudes are selected to achieve calculations of the partial derivatives which approach limit values. Due to round-off characteristics of the computer and the inability to achieve exactly converged responses, there is generally a practical limit to how small the various Δq_j values can be. Some care and experimentation are therefore warranted in the selection of the Δq_j perturbation levels.

GENERAL DESCRIPTION OF THE G400PA PROGRAM STRUCTURE

The G400PA Rotor Aeroelastics Analysis is an extended, special purpose version of the parent G400 analysis described in Reference 1. The G400 analysis was revised to include the dynamics of blade appended pendular vibration absorbers, and the additional blade loadings (both aerodynamic and dynamic) due to prescribed sinusoidal hub motion. This version includes impedance matrix calculations, teetered rotor simulation, spanwise variable airfoil data, direct coupling with the UTRC Rotor Inflow Analysis (UTRC Program F389) and the use of higher harmonic pitch control angles. The eigensolution and transient spectral stability analysis features are deleted in this version of G400. The program was coded in FORTRAN IV and developed on the UNIVAC 1110/81A computer system and has been converted to the IBM370 and Langley Research Center CDC systems.

Program Structure

The G400PA program is structured in a generally conventional hierarchical fashion with an initial routine (MAIN), appropriate modular levels and a collection of utility subroutines and/or functions. The subroutine calling structure is presented in the tabular outline given below; this functional structuring also serves to list the elements (subroutines and/or functions), contained in G400PA. Note that the hierarchical structure is alternately indicated using indentations with indicating symbols and/or nested parentheses: Note also that this table lists the subroutines in alphabetical order within any given hierarchical level and not with respect to calling order, size or importance. The subsection which follows Table I presents a brief description of each of the G400PA elements.

TABLE I

HIERARCHICAL LISTING OF G400PA ELEMENTS

● MAIN

■ NIAM

- ▲ BNDGTT (GJR, QUADFT)
- ▲ INISH2
 - ◆ ADMCOF
 - ◆ DPCHEK
 - ◆ PABSSU (ADMCOF)
- ▲ INTCOF (FACT12, LNAERO)
- ▲ LNAERO (BLIN5, SHLDM)
- ▲ LOAD
- ▲ MODEIN
- ▲ MYKSTD (GJR)
- ▲ PRNT
- ▲ PTFLLG
- ▲ RESETQ (QQPSET)
- ▲ SPNWIZ
- ▲ SPRINT
- ▲ TRFLX1
- ▲ TWOF

■ MOTION

- ▲ MAJITR
 - ◆ F389SU
 - ▼ BLIN5
 - ▼ INTERP
 - ▼ LNAERO
 - ▼ SHLDM
 - ▼ STALN
 - ◆ QSTHRM (HARM)
 - ◆ RESETQ (QQPSET)
 - ◆ TMARCH

TABLE I (Cont'd)

▼ ADAMS

▼ AERPRF (ALFCOR (HEYSDL(HEYSK)))

▼ BLADEL

◆ FACT12

◆ HBINRT

◆ HHCANG

◆ QQPSET

◆ RDHANL

◆ SETUP

◆ SPANS

● BLIN5

● DMPRTB

● HYSDMP

● SHLDM

● UNCOEF

▼ BLIN5

▼ LNAERO

▼ SHLDM

▼ STALM

▼ STALN

▼ ULSTAL

◆ TABLE

▼ CROUTS

▼ EXTRAP

▼ QPPTST

▼ STRSS

▼ TEETR (GJR)

● TRMRLB (GJR)

▲ HUBSUM

Brief Description of Program Elements

ADAMS

This function implements an algorithm for time integration of any of the time dependent variables.

ADMCOF

This subroutine evaluates the coefficients required for the time integration algorithm.

AERPRF

This subroutine completes the calculations for and outputs the summary of aerodynamic performance quantities.

ALFCOR

This subroutine calculates the corrected rotor angle-of-attack due to the proximity of a ground plane or wind tunnel walls using the theory of Reference 5.

BLADEL

This subroutine provides the computational loop over number of blades in forming the blade response equations. The upper limit on this loop is (1,2) depending on whether the rotor is of (unteetered, teetered) type.

BLIN5

This subroutine does a tri-variant table loop up of the airfoil section coefficients. The three variables are angle-of-attack, Mach number and spanwise station.

BNDGTT

This subroutine calculates the flatwise and edgewise bending stiffness characteristic of the torque tube component of a bearingless rotor, as required for the redundant analysis calculation (see RDANAL).

CROUTS

This subroutine is a compact simultaneous equations solver used for non-teetered rotor configurations. It uses the Crout Reduction method described in Reference 6.

DMPRTB

This subroutine does a table look-up to implement the nonlinear lag damper angular rate vs damper moment characteristics.

DPCHEK

This subroutine tests the input integration steps size for acceptable accuracy, and automatically decreases it if the value is too large.

EXTRAP

This subroutine effects a "static" solution on any degree-of-freedom whose natural frequency is sufficiently high to approximate the response neglecting the twice time differentiated term in that degree-of-freedom's governing equation.

FACT12

This subroutine performs an interpolation function calculation in the use of input tabulated variable inflow.

F389SU

This subroutine sets up the various blocks of data needed by the (UTRC F389) variable inflow branch of the coupled rotor/fuselage vibration analysis and writes them to appropriate data files. A detailed description of the appropriate data transmitted between the G400PA and F389 portions of the analysis is given in Reference 2.

GJR

This utility subroutine optionally obtains simultaneous equation solutions and/or matrix inversions using the Gauss-Jordan Reduction method.

HARM

This utility subroutine performs a Fourier (harmonic) Analysis of any time history string of data. This harmonic analysis uses a negative cosine and sine definition for the harmonic components.

HBINRT

This subroutine calculates components of inertial acceleration, as measured in the rotating blade coordinate system, from the prescribed harmonics of hub motion.

HEYSDL

This subroutine calculates interference factors needed for subroutine ALFCOR.

HEYSK

This subroutine calculates induced velocity functions for subroutine HEYSDL.

HHCANG

This subroutine calculates contributions to the total blade pitch angle and its first and second time derivatives accruing from higher harmonic control angle inputs.

HUBSUM

This subroutine provides a printout of the rotor hub loads and impedance matrix calculations which are transmitted to the coupled matrix/fuselage vibration analysis program.

HYSDMP

This subroutine calculates the increment to blade edgewise bending moment to account for hysteretic structural damping. This formation of structural damping is dependent on edgewise deflection and the signs of rate and acceleration, but not their magnitudes.

INISH2

This subroutine initializes arrays and logic variables, and nondimensionalizes parameters, as required for the time-history solution.

INTCOF

This subroutine forms the modal integration coefficients.

INTERP

This utility subroutine provides linear interpolation calculations for subroutine F389SU.

LNAERO

This subroutine calculates partial derivatives of airfoil section coefficients with respect to angle-of-attack and Mach number.

MAIN

This is the main program element. Its explicit functions are to input the tabulated airfoil section data and to call subroutines NIAM and MOTION.

MAJITR

This subroutine provides the structuring needed to produce a trimmed configuration, and to calculate the impedance matrices. Specifically, this subroutine provides the iterative loop structure to perturb various system parameters in a systematic manner to form numerical partial derivatives, both those needed for trim and those needed for the impedance matrices.

MODEIN

This utility subroutine inputs the blade bending and torsion mode shapes and their derivatives with respect to span.

MOTION

This subroutine controls the time-history solution flow.

MYKSTD

This subroutine calculates the static flatwise bending deflection and spanwise derivative distributions for the blade for unit load on the inboard and of the cantilever mounted torque tube (for bearingless rotor rotor applications only).

NIAM

This subroutine performs the following functions:

1. completes the input of the required data; specifically (a) the inertia, elastic, geometric and other operational data, (b) the blade mode shape data, (c) the variable inflow data, and (d) the saved initial conditions, from an appropriate data file.
2. performs some initializations and/or nondimensionalizations of logic and system parameters.
3. calculates the deflection correction arrays which accrue from structural twist.

PABSSU

This subroutine sets up parameters and provides appropriate nondimensionalizations as required for the prescribed hub motions and simulations of the pendular absorbers.

PRNT

This subroutine provides an echo print output of the Part II input data which pertains to the Inertia, Elastic, Geometric and other Operational Data.

PTFLLG

This subroutine calculates the parameters used to define the pitch-flat, pitch-edge and pitch-flap couplings.

QPPTST

This subroutine tests the system degrees-of-freedom for numerical instabilities. The criteria used to identify such an instability are the occurrence of three sign changes of increasing amplitude in three time steps.

QQPSET

This subroutine sets the blade modal responses and modal rates for a given blade from the vectors of system response amplitudes and rates, respectively.

QSTHPM

This subroutine performs harmonic analyses (using subroutine HARM) of the blade modal responses, pendular absorber responses, hub shears and moments, and blade stresses, after the responses have converged to periodicity.

QUADFT

This subroutine fits a quadratic function to any set of three ordinates corresponding to three equally spaced abscissae.

RDNANL

This subroutine makes the redundant analysis calculations needed for simulations of bearingless rotor configurations.

RESETQ

This subroutine places selected terminal conditions into an array and writes them to a data file for use as initial conditions for subsequent runs.

SETUP

This subroutine sets up the inertia coupling matrix and excitation vector for the modal responses of a given blade.

SHLDM

This subroutine analytically approximates the NACA 0012 airfoil aerodynamic coefficients as functions of angle-of-attack and Mach number.

SPANS

This subroutine implements the loop over spanwise station in forming the blade response equations. The spanwise inertia, aerodynamic and gravity load distributions are formed in this subroutine.

SPNWIZ

This function performs a numerical integration between blade section centers of a specific integrand type as required for forming the deflection corrections functions due to structural twist.

SPRINT

This subroutine outputs (as optionally requested) the spanwise integration coefficients. Although most of these coefficients were required only for the (deleted) eigensolution, some are used in the time-history solution. For completeness all coefficients were retained.

STALM

This function approximates the variation of static moment coefficient stall angle with Mach number for the NACA 0012 airfoil.

STALN

This function approximates the variation of static normal force (lift, to close approximation) coefficient stall angle with Mach number for the NACA 0012 airfoil.

STRSSS

This subroutine calculates the spanwise stresses and integrated hub loads optionally using the force-integration or mode deflection methods.

TEETR

This subroutine combines the inertia coupling matrices and excitation vectors for a two-bladed rotor to effect the teetered rotor boundary conditions at the blade roots.

TMARCH

This subroutine controls the solution flow for obtaining the time-history solutions. It furthermore tests for numerical instabilities and convergence to periodicity.

TRFLX1

This subroutine calculates the torsion deflection characteristics of the flexbeams (for bearingless rotor configurations) due to spanwise varying torques resulting from the concentrated shears and moments at junction point of the flexbeam, torque tube and blade proper.

TRMLB

This subroutine calculates the final partial derivative matrices used to obtain a trimmed flight condition.

TWOF

This function performs a least-square curve fit calculation on blade twist to facilitate subroutine NIAM in the numerical differentiation of blade twist.

ULSTAL

This subroutine performs a table lookup of the input airfoil data to obtain (1) derivatives of section unstalled lift and moment coefficients with respect to angle-of-attack, and (2) static lift and moment stall angles, for use in subroutine UNCOEF.

UNCOEF

This subroutine implements the UTRC synthesized, unsteady stalled airloads formulations, as described in Reference 7.

PROGRAM INPUT DESCRIPTION

The required input to the program consists of the following major data blocks in order of loading:

- I. Airfoil Data
- II. Inertia, Elastic, Geometric and other Operational Data (in Loader Format)
- III. Blade Mode Shape Data
- IV. Harmonics of Variable Inflow

Details for preparing the data for each of these blocks are given in the subsections which follow. An additional subsection provides information for facilitating program operation and improving its efficiency.

I. Airfoil Data

This data block generally consists of one or more sets of tables of two-dimensional lift, drag and pitching moment coefficients versus angle-of-attack for various Mach numbers for up to four (4) arbitrary spanwise locations. Additionally, if unsteady aerodynamics are used, the static stall angles and linear coefficient slopes for both lift and pitching moment are included in this table.

Input Format for First Card(s)

While actual set-up of this data block follows a basic format (described below), specific variations are required on the first card(s) of this block depending on optional usage. These variations denote whether multiple data sets are to be input for respective spanwise locations, a single set is to be input for use on all spanwise locations, or an analytic representation of the NACA 0012 airfoil is to be used for all spanwise locations. Each of these optional usages are described below.

Multiple Spanwise Airfoils

For the case of distinct airfoil characteristics being defined at up to four (4) multiple spanwise locations, the first card image format is as follows:

card #1A:

NZ NRCL NRCD NRCM TITLE(optional)

(4I2, A72)

where NZ would be ignored so long as the sum of the quantities NRCL, NRCD and NRCM is 4 or greater. The quantities NRCL, NRCD and NRCM are, respectively, the number of radial stations for which multiple c_l , c_d and $c_{mc}/4$ airfoil data are to be inputted, as appropriate, each with a minimum value of 1 and a maximum value of 4. Note that at least one of these three inputs must have a value of 2 or greater. For multiple spanwise section properties, an additional card, following the one described above, is then required, which begins the input of the c_l airfoil data:

card #1B:

NZ(1) RADCL(1) TITLE(optional)

(I2, F8.0, A70)

where NZ(1) is the number of Mach number for which groups of c_l data are to be read in for the first radial station; RADCL(1) is the nondimensional radial station at which the airfoil data is defined.

Single Airfoil Description

For the case of a single airfoil to be used for all spanwise locations, a single first card image is input. This card is similar to the card #1A described above, except the quantities NRCL, NRCD and NRCM are input as zero (or the columns are left blank):

card #1:

NZ(1) 0 0 0 TITLE(optional)

(4I2, A72)

In this case the card is interpreted as the first card of the c_l data with the RADCL(1) information omitted (see description above for card #1B).

Analytic Airfoil Description

For those optional cases wherein the analytic NACA 0012 airfoil option is invoked (see location 996 discussed in the following subsection) the first card image must be a single card with blank or zeroed columns 1 through 8. For this option, the remainder of the airfoil data block of data is omitted.

Input Format for Subsequent Cards

For those cases wherein tabulated airfoil data are to be input, the subsequent inputs continue the airfoil c_p data initiated with the #1A and/or #1B cards. Thus, the card image set-up defined below is then input NRCL times (or only once, if NRCL = 0):

card #2:

J N M A(1) CL(1) A(2) CL(2) ...A(4) CL(4) (12, 10F7.0)
--

cards #2+:

A(5) CL(5) ... (F9.0, 9F7.0)

•
•
•

...A(N) CL(N) ALSTAL DCLDAO (F9.0, 9F7.0)

where: J is the number of data entries to be input into each Mach number group. N is the number of angle-of-attack - c_p abscissae-ordinate pairs to be input. Normally a maximum of thirty-four (34) c_p , α pairs may be input; thirty-three (33) pairs are input if the unsteady option is chosen. M is the Mach number appropriate to the data group. A(i) are the N angle-of-attack abscissae in degrees and CL(i) are the N lift coefficient ordinates. ALSTAL and DCLDAO are, respectively, the static stall angle, in degrees, and the lift curve slope at zero angle-of-attack, in per degree; these items are needed only if the unsteady airloads option is invoked. Note that J is fixed-point formatted, but N and M are floating point formatted.

Cards 2 and 2+ are repeated for each successively higher Mach number. A maximum of 12 Mach numbers is allowed and the lowest and highest Mach numbers need not define the total working range as the search technique uses the boundary data for Mach numbers beyond the range input. Thus, repeated data for zero and supersonic Mach numbers are not needed. The lowest Mach number input must contain an angle-of-attack range from -180° to 180° or from 0° to 180° depending on whether or not unsymmetric airfoil data is being input; all higher Mach number data need extend only from -30° to 30° or from 0° to 30° in a similar manner.

The general format described above is repeated for the c_d and $c_{mc/4}$ subblocks in that order but with either card image #1B or #1A used, depending on whether multiple airfoil section data are or are not being input (and used). The static stall angles and aerodynamic coefficient curve slopes at zero angle-of-attack are deleted for the c_d subblock. Lastly, note that the total storage allocated for the combined airfoil data is 4000 (which is somewhat less than 2000 abscissa - ordinate point pairs). The maximum storage should be adequate for most applications and can be "budgeted" among the various spanwise sections, as appropriate.

II. Inertia, Elastic, Geometric and Other Operational Data

This data block includes those items used to define the more detailed dynamic features and/or those which are most likely to vary from case to case. The card image format for these data is as follows:

NN L DATA(L) DATA(L+1) ... DATA(L+4) (I2, I4, 5F12.0)

where: NN is the number of data items to be input on a given card; NN must not exceed 5. L is the location or identifying number of the first data item on the card columns 3 - 6 right adjusted. DATA(L+1) represents the various data items on the card image, columns 7-18, 19-30, 31-42, 43-54, and 55-66, in the floating point format. The locations or identifying numbers for the various data and control items are listed below along with definitions and other pertinent comments; note that some data locations are intentionally left blank.

<u>Location</u>	<u>Item</u>	<u>Description</u>
1	ΩR	Rotor tip speed, ft/sec.
2	R	Rotor radius, ft.
3	ρ	Air density, lb-sec ² /ft ⁴ .
4	a_∞	Speed of sound, ft/sec.
5	b	Number of blades.

<u>Location</u>	<u>Item</u>	<u>Description</u>
6	\bar{e}	Nondimensional offset distance of start of deformable and/or deflectable portion of rotor blade (hinge offset for articulated rotors), e/R .
7	B	Tip loss, used to define equivalent momentum area and three-dimensionality corrections to computed two-dimensional airloads near the blade tip.
8	NSEG	Number of blade segments used to define spanwise variable arrays.
9	$\Delta\psi$	Azimuth increment used in the numerical integration of the dynamic equations, deg. (See section on general information for efficient program usage.)
10	N_F	Number of "flap trials", i.e., maximum number of rotor revolutions for which the blade time-history will be computed in an attempt to obtain convergence to periodicity. If a transient response is desired for only a portion of one rotor revolution the program will compute a time-history solution for any nonzero fractional N_F value input. An identically zero value will cause the time-history solution to be by-passed entirely.
11	ϵ_F	Flapping tolerance to within which the aeroelastic/dynamic responses must repeat on successive revolutions in order for the motion to be considered converged to periodicity. The tolerance applied to lead-lag motion is equal to $5\epsilon_F$.
12	A_{1s}	Longitudinal cyclic pitch, coefficient of minus $\cos\psi$ term in Fourier expansion of blade control pitch angle, deg.
13	B_{1s}	Lateral cyclic pitch, coefficient of minus $\sin\psi$ term in Fourier expansion of blade control pitch angle, deg.
14	$\theta_{.75R}$	Blade collective pitch angle as defined at the 75% radius, deg.

<u>Location</u>	<u>Item</u>	<u>Definition</u>
15	λ	Mean rotor inflow ratio.
16	V	Forward flight velocity, kts.
17	σ	Rotor area solidity ($bc/\pi R$).
18	Δc_{d0}	Increment added to all values of c_d obtained from tabulated airfoil data or from the analytic NACA 0012 data. Airfoil data generally correspond to smooth wind tunnel models and Δc_{d0} is often used to adjust for the higher drag of production blades; a commonly used value of Δc_{d0} is 0.002.
19	(Control)	Make greater than zero (1.) for first case or when new <u>blade modal data</u> are to be input. Program automatically sets this control number to (-1.) after each loading of modal data.
20	$N_{\text{cut-out}}$	Number of blade segments, starting at inboard end and defining the cut-out region, for which the lift and moment coefficients are set to zero.
21	$(c_d)_{\text{cut-out}}$	The drag coefficient used on the first $N_{\text{cut-out}}$ segments.
22	θ_1	Built-in linear blade twist angle; i.e., difference between tip and root built-in angles, positive when tip angle is greater (L.D. up) than root angle, deg.
23	$\Delta\psi_{\text{print}}$	Azimuth increment used to present printed output of various pertinent aerodynamic, dynamic and elastic load distributions as well as aeroelastic responses and stresses, deg. This input quantity should be an integral multiple of location 9, deg.

<u>Location</u>	<u>Item</u>	<u>Description</u>
24	θ_{β}	"Direct" value of pitch-flap coupling ($\Delta\theta/\Delta\beta$). A nonzero value will suppress a calculation of this quantity from the input pitch-horn/push-rod geometry.
25	θ_{δ}	Pitch-lag coupling ($\Delta\theta/\Delta\delta$).
26	C_{LD}	Viscous lag damper coefficient, ft-lb-sec.
27	c	Blade chord if chord is constant, otherwise omit, ft.
28	NFM	Number of flatwise bending modes to be used (4 max).
29	NEM	Number of edgewise bending modes to be used (3 max).
30	NTM	Number of elastic torsion modes to be used (3 max) note that the total number of dynamic degrees-of-freedom is limited to 10. Thus, if the articulation degrees-of-freedom, β and/or δ , are used, or if the rigid feathering d.o.f. is invoked, NFM, NEM and NTM will be automatically changed to keep the total degrees-of-freedom to no more than 10.).
31-34	$\bar{\omega}_{w_i}$	Flatwise modal frequencies, nondimensional with respect to Ω , in ascending modal order.
37-39	$\bar{\omega}_{v_k}$	Edgewise modal frequencies, nondimensional with respect to Ω , in ascending modal order.
40-42	$\bar{\omega}_{\theta_j}$	Torsion modal frequencies, nondimensional with respect to Ω , in ascending modal order.
43	A_{2s}	Second harmonic cyclic pitch coefficient of minus $\cos 2\psi$ in Fourier expansion of blade control pitch, deg.
44	B_{2s}	Second harmonic cyclic pitch coefficient of minus $\sin 2\psi$ in Fourier expansion of blade control pitch, deg.

<u>Location</u>	<u>Item</u>	<u>Description</u>
45	g	Acceleration due to gravity, ft/sec ² ; a negative value implies inverted flight.
46	(Control)	Make nonzero (1.) if airfoil data for a <u>nonsymmetric airfoil</u> are to be used.
47	(Control)	Make nonzero (1.) if the total <u>(transient) time-history</u> is to be output; i.e., responses calculated before convergence to periodicity is obtained.
48	(Control)	Make nonzero (1.) if the <u>modal responses</u> and <u>hub shears and moments</u> are to be (negative) <u>Fourier analyzed</u> after periodicity has been obtained.
49	(GJ) _{root}	Torsional rigidity at the blade root, lb/ft ² .
50	K _θ _{root}	Torsional spring rate connecting root of blade to fixed structure to represent control system flexibility, ft-lb/rad. A nonzero value will automatically introduce the rigid-body feathering degree-of-freedom as an addition "torsion mode". Note that this "mode" will inherently couple with the NTM normal elastic torsion modes at frequencies both below and above the input torsion frequencies (locations 40-42); hence, a smaller integration interval will generally be required.
51	(Control)	Make nonzero (1.) to simplify the numerical <u>spanwise integration techniques</u> from the nominal trapezoidal rule to rectangular (Eulerian) form. Rectangular integration is effected by setting the quadrature numbers used for spanwise integration equal to the input segment lengths (loc. (100-114)). Use of this option is recommended for blade configurations with significant discontinuities in spanwise properties (e.g., counterweights, tip weight, step twists, etc.).

<u>Location</u>	<u>Item</u>	<u>Description</u>
52	(Control)	Make nonzero (1.) to output modal <u>integration constants</u> used in the eigensolution and, to a limited extent, in the time-history solution.
53	(Control)	Make nonzero (1.) to load (vorticity) <u>induced velocity distribution</u> either <u>from</u> cards or unit 14, as per location 999.
54	(Control)	Make nonzero (1.) to <u>use</u> the <u>induced velocities</u> loaded as per location 53.
55	α_s	Shaft angle-of-attack, deg. This input item serves a dual role: when variable inflow is used (either vorticity induced or Glauert momentum) α_s is used to define λ_{ram} . Also, when a major iteration is to be performed (nonzero location 60) and when trims on propulsive force are deactivated (zero location 59) the program will trim to this input shaft angle.
56	L_{req}	Requested value of lift to be used in major iteration, lb.
57	PF_{req}	Requested value of propulsive force to be used in major iteration, lb.
58	ϵ_{Lift}	Tolerance on lift for major iteration, lb. A zero value deactivates trimming on lift.
59	ϵ_{PF}	Tolerance on propulsive force for major iteration, lb. A zero value deactivates trimming on propulsive force. The automatic trim calculation (major iteration) must trim either to a required propulsive force or to a required shaft angle-of-attack; therefore a deactivation of trim to propulsive force automatically directs the trim calculation to trim to requested shaft angle, location 55.

<u>Location</u>	<u>Item</u>	<u>Definition</u>
60	N_{MI}	Maximum number of major iterations to be made in an attempt to achieve trim. A zero value will deactivate the major iteration; a negative value will activate a stall avoidance calculation if, when attempting to trim, the rotor becomes stalled. (See section on general information for efficient program usage.)
61	β_B	Built-in precone angle, deg. An identically zero value denotes a rotor blade articulated in flapping; similarly, a finite nonzero signifies a blade nonarticulated in flapping or a teetering rotor.
62	PM_{req}	Requested value of pitching moment for major iteration, lb-ft (positive nose up).
63	ϵ_{PM}	Tolerance on pitching moment for major iteration, lb-ft. A zero value deactivates trimming on pitching moment.
64	RM_{req}	Requested value of rolling moment for major iteration, lb-ft (positive port side up).
65	ϵ_{RM}	Tolerance on rolling moment for major iteration lb-ft. A zero value deactivates trimming on rolling moment.
66	(Control)	Trim derivative calculation option. Input (0., 1.) to calculate the <u>aerodynamic partial derivative matrices</u> (using linear strip theory, numerically).
67	β	Initial condition on articulated flapping or teetering angle, as appropriate, rad.
68	$\dot{\beta}$	Initial condition on (nondimensional) articulated flapping or teetering angle rate, as appropriate.
69	δ	Initial condition on articulated lead-lag angle, rad. (positive forward).

<u>Location</u>	<u>Item</u>	<u>Definition</u>
70	δ^* (δ)	Initial condition on (nondimensional) articulated lead-lag rate.
72	δ_B	Built-in prelead angle, deg. An identically zero value denotes a rotor blade articulated in lead-lag; similarly a finite nonzero value signifies a blade nonarticulated in lead-lag.
73	(Control)	Input nonzero (1.) to harmonically analyze and output <u>harmonics of flatwise stresses</u> .
74	(Control)	Input nonzero (1.) to harmonically analyze and output <u>harmonics of edgewise stresses</u> .
75	(Control)	Input nonzero (1.) to harmonically analyze and output <u>harmonics of torsional stresses</u> .
76	(Control)	Initial condition input control. Input (1., 2.) to (only write, both read and write) <u>response initial conditions</u> to unit 26. Note that an input value of 2. is typically used only for restart cases involving previous runs.
77	ψ	Initial condition on rotor azimuth, deg.
78	K_{vim}	Effectivity factor of the induced velocity calculated using actuator disk momentum considerations in calculating inflow angle at a local blade section. Default value is 1., corresponding to conventional usage of momentum actuator disk inflow. This input quantity can be used to approximate the effects caused by real inflow characteristics as modeled by more accurate theories. For such usage, the effectivity would typically be in the range of 1.0 \rightarrow 1.1.
79	(Control)	<u>Generalized Glauert</u> (momentum derived) <u>variable inflow</u> option. A zero value deactivates usage. A value of 1. causes the input induced velocity components to be used; a value of 2. causes the input values to be used initially, and then varied in trim calculations in place of control

<u>Location</u>	<u>Item</u>	<u>Definition</u>
		angles; a value of 3. causes the control and shaft angles to be fixed and the induced velocity components to be varied only to satisfy momentum equations in any requested major iteration. If the value is 1., the induced velocity components will be varied to satisfy momentum considerations in addition to the usual trim calculation.
80-82	$\bar{v}_o, \bar{v}_{1c}, \bar{v}_{1s}$	Initial conditions on the "momentum" induced velocity components comprising a Glauert-like variable inflow description. Note that the "vorticity" variable inflow (controlled by locations 53 and 54) and the momentum variable inflow can be used separately or simultaneously.
83	(Control)	Input (1.) for <u>teetered rotor configurations</u> .
84-89		<u>These input data pertain only to teetered rotor configurations (loc (83) = 1.)</u>
84	h_{usl}	Distance the hub vertex point is underslung below the teeter hinge, in.
85	β_1	Limit stop angle below which there is no constraint on teetering, deg. (a zero input is treated as infinity).
86	K_{β_1}	Initial limit stop flapping spring rate defined when β_1 limit stop is first reached, ft-lb/rad.
87	β_2	Saturation limit stop angle above which the limit stop constraint is defined by a second constant spring rate, deg.
88	M_{β_2}	Saturation moment when the β_2 limit stop is reached, ft-lb.
89	K_{β_2}	Flapping spring rate of limit stop for teeter angles in excess of β_2 , ft-lb/rad. (Note that locations 85-89 provide a general representation of a nonlinear limit stop spring.)

<u>Location</u>	<u>Item</u>	<u>Description</u>
93	$c_{d_{sf}}$	Blade airfoil section <u>skin friction drag coefficient</u> , for use with swept airfoil, skewed flow option.
94	ζ_{vse}	Critical (viscous) damping ratio used to approximate structural damping in edgewise bending modes.
95	(Control)	<u>Variable (vorticity) inflow shape option.</u> A value of (0., 1.) causes the input vorticity variable inflow azimuthal distributions to be used in a (continuous point-to-point, stepped pulse) manner.
96	(Control)	Make 1., to invoke the <u>radial flow swept airfoil</u> option.
97	$\theta_{1_{equ}}$	Linear equivalent blade (nonlinear) twist angle defined similar to location 22, deg. A nonzero value for $\theta_{1_{equ}}$ is required to use the input nonlinear twist arrays and is used to calculate that portion of the aerodynamic inflow velocity at the 3/4 chord position, U_p , accruing from radial flow and twist.
98	(Control)	Input nonzero (1.) for <u>stress calculations</u> using the mode deflection method. Zero value defaults to force-integration method.
99	(Control)	Location used to <u>end a case</u> or series of cases. Input (+1.) to end the Loader Format data block for the case defined by the Loader data and load additional cases at the conclusion of that case. Make (-1.) to end the Loader data and read no further cases. In both instances the word count, LL, (see beginning of this section above) should be (-1). <u>Note: this entry must appear singly on an input card, and that card must be the last card for the case.</u>

<u>Location</u>	<u>Item</u>	<u>Description</u>
100-114	Δx	Nondimensional blade segment lengths, in order from root to tip, maximum of 15 values, starting from the offset location. Accuracy is generally improved if the last segment is small (< 0.03).
115-129	M_i	Mass of each blade segment, lb-sec ² /ft.
130-144	θ_{Ba}	Aerodynamic built-in nonlinear twist angle distribution, deg. Since collective angle is defined at the 75% span location, θ_{Ba} should have a zero value at 75% span. Should the structural twist angle distribution differ from θ_{Ba} , the appropriate data must be loaded into locations 690-704; otherwise, θ_{Ba} will be used for both aerodynamic and structural applications. Nonlinear twist distributions will be used only if a nonzero value is input into location 97, θ_{1equ} .
145-159	c_i	Blade chord at center of each blade segment (use for nonconstant chord blades only), root to tip, ft.
160-174	K_F	Constants relating (nondimensional) flatwise second derivative to flatwise stress $(Ec/R)_F$, evaluated at center of each segment, root to tip, psi.
175-189	K_E	Constants relating (nondimensional) second derivative to edgewise stress $(Ec/R)_E$, root to tip, psi.
190-204	τ/M	Constants relating torsional moment to torsional stress, root to tip, in ⁻³ .
205-219	\bar{k}_{z10}	Chordwise mass radii of gyration of blade segments about elastic (reference) axis, root to tip, nondimensional with respect to R.

<u>Location</u>	<u>Item</u>	<u>Description</u>
220-234	\bar{k}_{y10}	Thicknesswise mass radii of gyration of blade segments about axis perpendicular to chord line and through the reference axis, root to tip, nondimensional with respect to R.
235-249	\bar{k}_A	Area radii of gyration about elastic axis, root to tip, nondimensional with respect to R.
250-264	$\bar{y}_{10c/4}$	Distances from elastic axis forward to airfoil quarter chord position, root to tip, nondimensional with respect to R.
265-279	\bar{y}_{10CG}	Distances from elastic axis forward to airfoil section mass centers, root to tip, nondimensional with respect to R.
280-303	-	<u>Initial conditions on the elastic modal responses for the reference blade.</u>
280-283	q_{wi}	Initial conditions on i'th flatwise bending mode deflections.
286-289	$^*q_{wi}$	Initial conditions on i'th flatwise bending mode (nondimensional) rates.
292-294	q_{vk}	Initial conditions on k'th edgewise bending mode deflections.
295-297	$^*q_{vk}$	Initial conditions on k'th edgewise bending mode (nondimensional) rates.
298-300	$q_{\theta j}$	Initial conditions on j'th torsion mode deflections.
301-303	$^*q_{\theta j}$	Initial conditions on j'th torsion mode (nondimensional) rates.
310-333	-	<u>Initial conditions on the elastic modal responses for the second blade of a teetered rotor configuration, in same order as locations 280-303.</u>

<u>Location</u>	<u>Item</u>	<u>Description</u>
355-369	Λ_s	Aerodynamic built-in sweep angle distribution, positive aft, deg.
498	NLDATT	Segment number of the lag damper (outboard) attachment point. Default value is 1.
499	(Control)	Input (0., 1.) as the <u>outboard lag damper attachment</u> is (inboard, outboard) of the feathering bearing.
500	(Control)	Input (1.) to use <u>tabulated lag damper moment vs. angular velocity properties</u> .
501	N_{LD}	Number of abscissa-ordinate pairs used to define the lag damper moment-angular velocity characteristics. Maximum of 24 pairs are allowed.
502-549		Table of lag-damper characteristics taken in point pairs: $(A_k), M(A_k)$; $U(A) = \text{rad/sec}$; $U(M) = \text{ft-lb}$. (Normal sign convention is that A and M have the same sign.)
554	(Control)	In general, a nonzero value invokes the <u>hysteretic (nonviscous) structural damping formulation</u> in the edgewise bending mode equations. Specifically, make (1., 2.) to use (the constant location 94 value, a spanwise distribution of values) in this nonviscous formulation.
559-569	ζ_{vse}	Distribution of edgewise nonviscous structural damping ($= 1/2 g_v$, where g_v is the usual structural damping coefficient).
600-614	$(I/c)_E$	Section moduli for flatwise bending, root to tip, in ³ . Note that the products of $(I/c)_F$ and K_F (locations 160-174) must equal the bending stiffness distribution, EI/R .
615-629	$(I/c)_E$	Section moduli for edgewise bending, root to tip, in ³ . See remarks above for flatwise bending section moduli.

<u>Location</u>	<u>Item</u>	<u>Description</u>
660-674	EB ₁	Torsional stiffness (to be multiplied by twist rate squared), as defined in reference 8, lb-ft ⁴ .
675-689	EB ₂	Torsion to edgewise elastic coupling stiffness (to be multiplied by twist rate), as defined in reference 8, lb-ft ³ .
690-704	θ_B _S	Structural built-in nonlinear twist angle distribution, root to tip if different from aerodynamic twist, deg. See remarks above for aerodynamic built-in twist, location 130-144.
705-719	$\Delta\theta_B$	Built-in (structural) twist angle change per segment length distribution, root to tip deg. Note that this item is a direct statement of the built-in twist rate distribution, θ'_B ; if all values of this distribution are input as zero, the twist rate distribution is computed internally using numerical methods from the input twist angle distributions, locations 130-144 or 690-704, as appropriate.
720-734	\bar{e}_A	Distances from reference (elastic) axis forward to edgewise bending neutral axis, root to tip, nondimensional with respect to R.
735-744	D _{FB}	Flexbeam plate bending stiffness distribution, lb-ft. Note that all items in locations 735-824 are required only for a redundant analysis of the torque-tube (flexbeam span of bearingless rotor (CBR) configurations) (see location 991).
745-754	GJ _{FB}	Flexbeam torsion (St. Venant) stiffness distribution, lb-ft ² .

<u>Location</u>	<u>Item</u>	<u>Description</u>
755-764	C_{FB}	Flexbeam section width (chord) distribution, ft.
765-774	$(EI_y)_{TT}$	Torque tube flatwise bending stiffness distribution, lb-ft ² .
775-784	$(EI_z)_{TT}$	Torque tube edgewise bending stiffness distribution, lb-ft ² .
785-794	M_{TT_i}	Mass of each torque tube segment whose span is defined by location 100-109, lb-sec ² /ft.
795-804	$(\bar{y}_{10_{CG}})_{TT}$	Distances from reference axis forwarded to torque tube mass centers whose masses are given in locations 785-794, nondimensional with respect to R. (Input locations provided, but quantity is not used.)
805-814	$(I/c)_{FTT}$	Section moduli for torque tube flatwise bending, in ³ . (Input locations provided, but quantity not used.)
815-824	$(I/c)_{ETT}$	Section moduli for torque tube edgewise bending, in ³ . (Input locations provided, but quantity not used.)
850-881	[T]	Trim partial derivative matrix, (obtained as output from a previous trim calculation. Nonzero values will suppress internal recalculation of [T].
900	N_{pend}	Number of blade appended pendular vibration absorbers activated, maximum of 2.
900-910	-	<u>Data for pendular absorber No. 1.</u>
901	r_{PAH}	Radial location of pendular absorber hinge attachment, in.
902	$z_{10_{PAH}}$	Location of pendular hinge point in direction normal to the section chord, (+ upward), in.
903	l_p	Pendular absorber arm length (i.e., distance from hinge point to mass center), in.

<u>Location</u>	<u>Item</u>	<u>Description</u>
904	M_{PA}	Mass of pendular absorber, lb-sec ² /ft.
905	I_P	Rotary inertia of pendular absorber about the hinge point, lb-sec ² -ft.
906	K_P	Discrete rotary spring restraining the pendular absorber about the hinge point, ft-lb/rad.
907	C_P	Rotary damping about hinge point, lb-sec-ft.
908	S_P	Frictional moment about the hinge point, lb-ft.
909	$\beta_P^{(1)}$	Initial condition on pendular absorber flap angle, rad.
910	$\beta_P^{*(1)}$	Initial condition on pendular absorber (nondimensional) flap rate, rad.
911-920	-	Repeat of locations 901-910, but <u>for the second pendular absorber</u> .
921-922	ω_{PA}	Integration frequencies for the pendular absorbers 1 and 2, respectively. These frequencies should be close to the respective natural frequencies of the absorbers. Default values are calculated from the input mechanical properties, nondimensional.
923-924	θ_{OPA}	Built-in (+, nose up) pitch angles, relative to section chord line for pendular absorbers 1 and 2, respectively, deg.
925-928	-	Initial conditions for the <u>pendular absorbers of the second blade</u> of a teetered rotor.
925-926	$\beta_P^{(2)}, (\beta_{P1}^{*(2)})$	Initial conditions for pendular absorber No. 1 (same as locations 909 and 910, but for second blade), rad.

<u>Location</u>	<u>Item</u>	<u>Description</u>
927-928	$\beta_{p2}^{(2)}, \beta_{p2}^{*(2)}$	Initial conditions for pendular absorber No. 2 (same as locations 919 and 920, but for second blade), rad.
930-939	-	Input data for controlling the calculations of the <u>hub excitation vector and the impedance matrix</u> .
930	m	Multiple of number of blades to determine the harmonic of hub motion and resulting loads and impedance. Thus, resulting frequency, ω , would be $\omega = mb\Omega$.
931	$\Delta\alpha$	Perturbational amplitude used for incrementing each of the components of linear hub acceleration (\ddot{x}, \ddot{y} and \ddot{z}) to calculate the impedance matrix numerically, ft/sec ² .
932	$\Delta\alpha$	Perturbational amplitude used for incrementing each of the components of angular hub acceleration ($\ddot{\theta}_x, \ddot{\theta}_y, \ddot{\theta}_z$) to calculate the impedance matrix numerically, rad/sec ² .
933	NSTAVB	Number of blade radial stations for which harmonics of vibratory stresses are to be included in augmented impedance matrix, maximum of 3.
934-936	ISTAVB	The (NASTAVB) radial station segment numbers for utilizing vibratory stresses in the augmented impedance matrix.
939	(Control)	Input (1.) to include <u>vibratory push-rod loads</u> in the augmented impedance matrix.
940-945	-	<u>Higher harmonic control pitch angle amplitudes</u> wherein the frequencies are at (b-1), (b) and (b+1) times the rotor rotational speed and b, the number of blades, is location 5, and where a negative Fourier Series representation is assumed.

<u>Location</u>	<u>Item</u>	<u>Description</u>
940-941	$A_{(b-1)s}, B_{(b-1)s}$	Cosine and sine components of (b-1) per rev higher harmonic control pitch angles, respectively, deg.
942-943	A_{bs}, B_{bs}	Cosine and sine components of (b) per rev higher harmonic control pitch angles, respectively, deg.
944-945	$A_{(b+1)s}, B_{(b+1)s}$	Cosine and sine components of (b+1) per rev higher harmonic control pitch angles, respectively, deg.
946	$\Delta\theta_{HHC}$	<u>Perturbational amplitude used for incrementing the components of higher harmonic control</u> (locations 940-945) to calculate the augmented impedance matrix numerically, deg. A zero value will retain the input higher harmonics of pitch control, but will suppress this portion of the impedance matrix calculation.
957	h	Height of positively thrusting rotor from ground or wind tunnel floor for purposes of evaluating Heyson corrections to rotor angle of attack (see Ref. 5), ft.
958	H_{WT}	Height of wind tunnel test section for purposes of evaluating Heyson corrections, ft. Note that zero values for the wind tunnel test section dimensions implies that ground effect corrections, rather than wind tunnel wall corrections, are to be made.
959	W_{WT}	Width of wind tunnel test section for purposes of evaluating Heyson corrections, ft.
975	CASE	Case number.
976	θ_{BPR}	Built-in elevation angle of push-rod attachment point, measurable when $\theta_{.75} = 0$, deg.
977	NDEL3I	Segment number of inboard attachment point of pitch input structural members (pitch horn, feathering cuff or torque tube) to blade spar.

<u>Location</u>	<u>Item</u>	<u>Description</u>
978	NDEL30	Segment number of outboard attachment point of pitch input structural member to blade spar. Note that if this structural element is attached to the blade spar at a single point (cantilevered configuration) NDEL31 and NDEL30 must both be input with the same appropriate value. For bearingless rotor (CBR) applications NDEL30 serves the additional function of defining the outer limit of the flexbeam; this limit is taken as the inner boundary of the NDEL31'th segment.
979	r_{PR}	Radial location (blade station) of push-rod to pitch input structural member attachment point, in.
980	$y_{10_{PR}}$	Location, forward of feathering axis, of push-rod to pitch input structural member attachment point, in. Note that input items 977-980 together with the input modal data provide the geometric data from which pitch-flap, pitch-flat and pitch-edge coupling are calculated. These calculations are bypassed if either of locations 978 or 980 are input identically zero.
981	NSPSTR	Segment number of innermost end of the feathering flexure; defaults to 1.
982	$\theta_{B_{FB}}$	Built-in twist angle of the flexbeam, positive leading edge up at outboard end of flexbeam, deg. Note that $\theta_{B_{FB}}$ is defined relative to the inputted twist angle distribution, which in turn is defined for zero collective angle. Thus, $\theta_{B_{FB}}$ represents the built-in collective angle for the blade.
983	\overline{GJ}_{FB}	(Inverse) averaged torsional stiffness of the flexbeam lb-ft ² .
984	$k_{T_{FB}}$	Equivalent or critical torsion stress coefficient for flexbeam; i.e., stress per unit average torsion strain as defined by total flexbeam twist, in-psi.

<u>Location</u>	<u>Item</u>	<u>Description</u>
985	(Control)	Make nonzero (1.) to include the " <u>wobble</u> " mode for cantilever torque tube configured bearingless rotors.
986	(Control)	When finite <u>snubber stiffnesses</u> are input (locations 987 and 988), the stiffness <u>alignments</u> (principal axes) are assumed to be (vertically and horizontally, in torque tube flatwise and edgewise directions) as location 986 is (0., 1.).
987	$K_{sz5} (K_{SF})$	Snubber vertical (torque tube flatwise) spring rate, lb/ft.
988	$K_{sy5} (K_{SE})$	Snubber horizontal (torque tube edgewise) spring rate, lb/ft.
989	(Control)	When the torque tube flexbeam redundant analysis is involved (location 991) the <u>torque tube</u> is assumed to be in (<u>tension</u> , <u>compression</u>) as location (989) is (0., 1.).
990	NTQTB1	Segment number of innermost end of torque tube; defaults to 1.
991	(Control)	Input nonzero (1.) to <u>activate the redundant analysis</u> option. When the redundant analysis is activated, the flexbeam and torque tube stiffness and mass inputs, locations (735) through (794), must be appropriately nonzero.
992	(Control)	Used to weight the effectiveness of nonlinear <u>ΔEI bending excitation of torsion</u> over the flexbeam span; the effectiveness is taken to be (100%, 0%, 100% (x) pseudo-torsion mode shape) as LOCATION (992) is (0., 1., 3.)).
993	Λ_{FB}	Flexbeam aspect ratio parameter ($= \frac{S}{C} \sqrt{1.5(1-\nu)}$) to determine plate-like deflection for torsion "pseudo-mode". A zero value gives a rod-like deflection shape.

<u>Location</u>	<u>Item</u>	<u>Description</u>
994	K_{WOB}	Spring rate of rotational spring connecting outboard end of torque tube to the blade spar about chordwise axis, ft-lb/rad. A zero value implies zero stiffness for pinned-pinned torque tube configurations and infinite stiffness for snubbed configurations.
995	K_{VOB}	Spring rate of rotational spring connecting the outboard end of the torque tube to the blade spar about an axis perpendicular to the chord line, ft-lb/rad (see above).
996	(Control)	<u>Analytic (static) airfoil option.</u> Make nonzero (1.) to use the built-in analytic approximation to the static NACA 0012 airfoil data.
997	(Control)	<u>Unsteady airfoil data option.</u> Make nonzero ($\geq 1.$) to use the synthesized unsteady airfoil data technique described in Reference 7. This can be used with either the explicit input airfoil data or the built-in analytic NACA 0012 static airfoil data. For nonzero values greater than unity, the "cutoff Mach number" (Mach number above which the unsteady data is disregarded in favor of quasi-static data) is taken to be the input value minus one (1.) rather than the built-in default value of 0.6. However, only nonstandard cutoff Mach numbers between 0.1 and 0.95 are accepted.
998	$\Delta\psi_{F389}$	Aximuth increment used to generate punched card image output which is then used as input data to UTRC Program F389 for computing variable inflow. This option is bypassed with a (0.) input value.
999	(Control)	Input (0., 1.) for data transferrals with the F389 variable inflow program to be made using (punched cards, data files). If data files are used, G400PA reads from unit 14, and writes to units 16, 23 and 13 .

<u>Location</u>	<u>Item</u>	<u>Description</u>
1000	(Control)	Input nonzero (1.) to activate use of the <u>tabulated time-histories</u> of incremental control angles.
1001	$N\Delta\theta_{.75}$	Number of abscissa-ordinate point pairs used to define time-history of $\Delta\theta_{.75}(t)$; calculation of this time-history is bypassed with a (0.) value.
1002-1050	$\Delta\theta_{.75}$	Table of $\Delta\theta_{.75}$ abscissa-ordinate point pairs; $U(\Delta\theta_{.75}) = \text{deg.}$; $U(t) = \text{sec.}$
1051	$N\Delta A_{1s}$	Number of abscissa-ordinate point pairs used to define time-history of $\Delta A_{1s}(t)$; zero value bypasses calculation.
1052-1100	ΔA_{1s}	Table of ΔA_{1s} abscissa-ordinate point pairs; $U(A_{1s}) = \text{deg.}$; $U(t) = \text{sec.}$
1101	$N\Delta B_{1s}$	Number of abscissa-ordinate point pairs used to define time-history of $\Delta B_{1s}(t)$; zero value bypasses calculation.
1102-1150	ΔB_{1s}	Table of ΔB_{1s} abscissa-ordinate point pairs; $U(B_{1s}) = \text{deg.}$; $U(t) = \text{sec.}$

Last Card Image for Block II (Loader) Data:

<div style="display: flex; justify-content: space-between;"><div><div style="display: flex; align-items: center;"><div style="margin-right: 10px;">-1 99 ± 1.</div><div style="margin-left: 10px;"><div style="display: flex; align-items: center;"><div style="margin-right: 5px;">↑</div><div style="display: flex; flex-direction: column; align-items: center;"><div style="margin-bottom: 5px;">+</div><div style="margin-bottom: 5px;">-</div></div></div></div><div style="margin-left: 10px;">other cases follow preceeding data defines last case</div></div></div><div style="text-align: right;">(I2, 14, F12.0)</div></div>

III. Blade Mode Shape Data

Included in this data are the radial distributions of the blade (uncoupled) flatwise, edgewise and torsion normal mode shapes and their derivatives. These quantities must generally be provided from an external source such as United Technologies Corporation Program E159 or an equivalent, in the following card image format:

NFM NEM NTM NSEG	(4I4)
------------------	-------

subsequent cards:

F(I) F(I+1) F(I+2) F(I+3) F(I+4)	(F18.0, 4F12.0)
----------------------------------	-----------------

where: NFM, NEM, and NTM are, respectively, the numbers of flatwise bending, edgewise bending and torsion normal modes whose mode shapes and derivatives are to be input. NSEG is the number of blade spanwise stations for which the input modal data are defined. F(i) are the modal functions listed below (defined at the i'th spanwise stations). Five entries per card are made for each F function input for NSEG total entries. The modal functions must be loaded in the following order:

γ_{w1}	(NSEG values, root to tip)	}	(NFM flatwise modes)
γ'_{w1}	(" " " " ")		
γ''_{w1}	•		
γ_{w2}	•		
•	•		
•			
γ_{v1}		}	(NEM edgewise modes)
γ'_{v1}			
γ''_{v1}			
γ_{v2}			
•			
•			
$\gamma_{\theta1}$		}	(NTM torsion modes)
$\gamma'_{\theta1}$			
$\gamma_{\theta2}$			
•			
•			

IV. Variable Harmonic Inflow

If location 53 of the Loader block of operational data is nonzero, the following block of variable harmonic inflow is loaded in:

card #1:

NHARML	(I3)
--------	------

card #2:

XLAMO(I)	(F14.0)
----------	---------

card #3:

XLAMC(I,1) XLAMC(I,2) ...	(5F14.0)
---------------------------	----------

card #3 + (NHARML/5):

XLAMS(I,1) XLAMS(I,2) ...	(5F14.6)
---------------------------	----------

NHARML is the number of harmonics of inflow to be loaded, and XLAMO(i), XLAMC(i,n) and XLAMS(i,n) are, respectively, the zeroth, n'th cosine and n'th sine components of harmonic inflow at the i'th radial station, wherein a positive Fourier series is assumed. The inflow is defined positive up and has the units of ft/sec. If $n > 5$ card image #3 is repeated until n cosine coefficients are input. The series of card images, #1 through #3+ are then repeated for the remainder of the NSEG segments.

V. Multiple Case Runs

The above described data set-up defines the correct ordering of required data blocks for a general case. When multiple cases are run (while remaining within the G400PA branch of the base program) the second and subsequent cases utilize most of the data input for the first case. The following rules apply to the running of multiple cases:

1. Airfoil data is loaded only for the first case; all subsequent cases within the run use the same tabular data, if analytic data is not used.
2. Only those items within the operational (Loader) data which are to be changed from case to case need to be input.
3. Item 99 of the operational data controls the running of subsequent cases; a (+1.) value causes a subsequent case to be loaded whereas a (-1.) value terminates the computer run after the current case.
4. Unless otherwise specified (by a +1. value for operational data item 19) the input modal array data block is used for all cases within the run.
5. Similarly, unless otherwise specified (by a +1. value for operational data item 53) the input harmonic variable inflow data block is used for all cases within the run.
6. Operational data items 19 and 53 discussed above are both automatically set to zero at the conclusion of the data input for every case.
7. Terminal conditions on the blade azimuth angle, item 77, and on the degrees-of-freedom, items 67-70, 280-303, 310-333, 909, 910, 919, 920, and 925-928, for any case are carried over as initial conditions on these quantities for the subsequent case. Thus, for some applications, e.g., investigations of unstable responses, it would be appropriate to reinitialize these items on the subsequent cases.

When solution flow leaves the G400PA branch of the base program, the ability to carry over terminal conditions (as initial conditions for a subsequent case) and/or any other quantities associated with trim is lost. However, a need still exists for preserving these initial conditions for subsequent reentries to the G400PA branch of the program. As per loader locations (76) (described above) these initial conditions are written to and read from file 26.

General Information to Facilitate Operation of Program and Improve Efficiency

Aside from considerations of the actual aeroelastic parameters describing the blade configuration, which are covered in the above sections, additional attention should be paid to the mechanics of obtaining efficient numerical solutions of the dynamic equations. In this regard, there arise two basic areas of concern wherein this section should be of assistance. The first of these areas is the proper selection of parameters for efficient temporal numerical integration of the dynamic equations (flapping or minor iterations) and the second is the proper selection of parameters for effecting a satisfactory rotor trim (major iteration). The following subsections provide information for making proper parameter selection in each of these areas.

Temporal Numerical Integration

As discussed in Reference 1 temporal integration of the higher differentiated response variables to obtain the lower ones is achieved in the G400PA program using a variant of the Adams integration algorithm. The selected algorithm is defined by means of the azimuthal integration step size, $\Delta\psi$, and the integration frequency, ω .

The integration step size should be an integral divisor of 360; a proper choice depends on the maximum coupled frequency inherent in the various aeroelastic responses. A reasonable upper limit for $\Delta\psi$ is 30 divided by the maximum such frequency in per rev. Values of $\Delta\psi$ greater than this upper limit will compromise the integration accuracy and, for sufficiently large values, will cause the computed responses to develop "numerical" instabilities. As a corollary, a check on any response which is predicted to be unstable by the analysis, is to rerun the case with a reduced integration step size to test for the possibility of the unstable response being merely a numerical instability.

For each response degree-of-freedom a different integration frequency, ω , is used in the integration algorithm; this frequency is, for each of the elastic modes, the respective input natural frequencies (locations 31-34, 37-39, and 40-42). The usual pendular frequencies of a rotating, hinged, rigid beam are taken as the integration frequencies of the flapping and lead-lag degrees-of-freedom. In addition to defining modal stiffnesses and integration frequencies, the input frequencies serve yet another purpose. As noted above, the proper value of integration step size, $\Delta\psi$, varies inversely with the maximum modal frequency. Thus, run times (caused by reduced step size) will significantly increase as any one modal frequency increases. Since any degree-of-freedom exhibiting a large natural frequency tends to respond quasi-statically, i.e., as if the acceleration (\ddot{q}) term were

negligible, a reasonable approximation to the response calculation is to avoid the numerical integration of the q term entirely and treat the response quasi-statically. This option can be invoked for any such high-frequency mode by input of a negative frequency; a negative sign will not affect the proper usage of the frequency in the calculation of the dynamic equations. Note that this optional response calculation can be invoked singly or in combination for any of the elastic modal responses (negative values in any of locations 31-34, 37-42, 921 and 922).

Hub Force and Moment Trim

Operation of the trim or major iteration feature of the program is controlled by input locations 55 through 60, 62 through 66 and, for some applications, 79. The main control for the major iteration is location 60, the number of major iterations, N_{MI} . A zero value causes the major iteration feature to be completely deactivated. On the basis of past usage, a reasonable range for this input appears to be from 5 to 10, depending on the tightness of the convergence tolerances selected and the "goodness" of the initial guesses on the control parameters. Convergence of the major iteration is adversely affected by any lack of convergence of the responses to periodicity within each trim iteration and by incursion of the rotor into a significantly stalled flight regime. Note that a negative value of N_{MI} will activate a stall avoidance calculation wherein the controls will be perturbed to reachieve unstalled flight rather than to achieve the prescribed trim condition. Should a major iteration fail to converge within any one run the last used control angles and initial conditions on response variables are generally available in output card image form and/or partially in the output printed records of each major iteration for use in subsequent major iterations.

An additional capability available for achieving a trimmed configuration is the option to calculate the aerodynamic partial derivative matrix either approximately using simple linearized strip theory or using a straightforward numerical differentiation. This option is controlled by loader location 66. It should be noted that the accuracy of the numerical differentiation is dependent upon how well the responses have converged to periodicity, which in turn is controlled by the flapping tolerance, loc. 11. When numerical derivatives are calculated, they are output on card images for subsequent input, using loader locations 850-881.

The trim iteration is operationally flexible as to what hub loads it will drive to requested values. Generally, the various requested hub loads, lift, propulsive force, pitching and rolling moment are activated in turn by specifying nonzero values for each of their respective tolerances. Specifically, the following table describes the optional combinations of hub loads and rotor shaft angle available with the G400PA trim capability.

TABLE II
SUMMARY OF OPTIONAL BASIC TRIM COMBINATIONS

Option	Lift	Prop. Force	Pitch. Moment	Roll Moment	$\theta_{.75R}$	A_{1s}	B_{1s}	α_s
1	S	U	U	U	V	F	F	S,(V)
2	S	S	U	U	V	F	F	V
3	U	U	S	S	F	V	V	S,(V)
4	S	U	S	S	V	V	V	S,(V)
5	S	S	S	S	V	V	V	V
6	U	U	S	U	F	V	F	S,(V)
7	S	U	S	U	V	V	F	S,(V)
8	S	S	S	U	V	V	F	V

where: F: Control parameter kept fixed
V: Control parameter varied
S: Trim parameter specified and trimmed to
U: Trim parameter unspecified and ignored

Note that for each option available, the individual trim parameter is activated by input of a positive, nonzero value for the respective parameter tolerance. For each option the trim calculation trims either to the specified propulsive force or the input shaft angle, α_s (location 55) as the propulsive force tolerance, c_{PF} , is finite or zero, respectively. A reasonable choice of tolerance values for the hub force and moment loads can be obtained from considerations of the helicopters inertia properties and acceptable deviations of the load factor from unity, and of the pitching and rolling accelerations from zero.

The trim calculation can also be used in conjunction with the Glauert variable inflow. Location 79 controls the use of this simplified form of variable inflow. A variety of trim calculation operations are achieved when this control location is nonzero. If this control option is 1., the Glauert variable inflow induced velocity components \bar{v}_o , \bar{v}_{lc} , and \bar{v}_{ls} (locations 80-82) would be varied in addition to those parameters shown in Table II to effect momentum balances in thrust, pitching moment, and rolling moment as well as the specified trim. If the control option is 2., only the velocity components would be varied (instead of the control angles, θ_{75R} , A_{ls} , and B_{ls}), but in an analogous manner. If the control option is 3., the trim calculation would again only vary the velocity components, but to achieve momentum balance only, with an specified trim.

PROGRAM OUTPUT DESCRIPTION

The complete printed output generated by the G400PA program can be classified into the following four major categories:

- I. Listing of Input Data
- II. Parameters Calculated from the Input Data
- III. Results of Time-History Solution
- IV. Impedance Matrices

This section describes the pertinent output pages associated with each of these categories. It should be noted that while output will always be generated for the first three categories, output for the remaining category depends upon the optional calculation of these impedance matrices. The subsections which follow describe, in turn, the details of each of these four categories.

Listing of Input Data

Output in this category includes a listing of the static airfoil data (if any is inputted), a descriptive listing of the "inertia, elastic, geometric and other operational" (Loader Format) data, and a listing of the harmonic variable inflow: blocks I, II, and IV, respectively, of the input data. If static airfoil data is inputted, then a listing of this data will be outputted for c_l , c_d and $c_{m_c}/4$ each with the format shown in Sample Page 1 where each column represents data at one Mach number. Within each column the first line gives the number of angle-of-attack/aerodynamic coefficient pairs defining the functionality; the second line is the Mach number, and the ensuing line pairs are the angle-of-attack/aerodynamic coefficient pairs, where the angles-of-attack are in degrees. This output closely follows the input format described in the previous section.

A description of the Loader Format data output is omitted herein since this output merely duplicates the description already given in even greater detail in the previous section. In Sample Page 2 is shown the listings of the inputted harmonic variable inflow, both by harmonic components and by azimuthal variation for each of the (maximum of) fifteen blade segments. As with the input format, the inflow is defined positive up, has the units of ft/sec and a conventional positive Fourier series representation is used.

Parameters Calculated from the Input Data

Sample Pages 3 and 4 list a variety of intermediate parameter calculations which, for the most part are directly applicable only to the composite bearingless rotor. Sample Page 3 presents the matrices and vectors used to define, respectively, the

CL TABLE

XX.X	YY.Y	ZZ.Z	AA.A	BB.B	CC.C	DD.D	EE.E	FF.F	GG.G	HH.H	II.I
.XXXX	.YYYY	.ZZZZ	.AAAA	.BBBB	.CCCC	.DDDD	.EEEE	.FFFF	.GGGG	.HHHH	.IIII
XXX.XXXX	XXX.XXXX	XX.XXXX	XX.XXXX	XX.XXXX	XX.XXXX	XX.XXXX	XX.XXXX	XX.XXXX	XX.XXXX	XX.XXXX	XX.XXXX
.XXXXXX	.XXXXXX	.XXXXXX	.XXXXXX	.XXXXXX	.XXXXXX	.XXXXXX	.XXXXXX	.XXXXXX	.XXXXXX	.XXXXXX	.XXXXXX
XXX.XXXX	XXX.XXXX	XX.XXXX	XX.XXXX	XX.XXXX	XX.XXXX	XX.XXXX	XX.XXXX	XX.XXXX	XX.XXXX	XX.XXXX	XX.XXXX
.XXXXXX	.XXXXXX	.XXXXXX	.XXXXXX	.XXXXXX	.XXXXXX	.XXXXXX	.XXXXXX	.XXXXXX	.XXXXXX	.XXXXXX	.XXXXXX
XXX.XXXX	XXX.XXXX	XX.XXXX	XX.XXXX	XX.XXXX	XX.XXXX	XX.XXXX	XX.XXXX	XX.XXXX	XX.XXXX	XX.XXXX	XX.XXXX
.XXXXXX	.XXXXXX	.XXXXXX	.XXXXXX	.XXXXXX	.XXXXXX	.XXXXXX	.XXXXXX	.XXXXXX	.XXXXXX	.XXXXXX	.XXXXXX
XXX.XXXX	XXX.XXXX	XX.XXXX	XX.XXXX	XX.XXXX	XX.XXXX	XX.XXXX	XX.XXXX	XX.XXXX	XX.XXXX	XX.XXXX	XX.XXXX
.XXXXXX	.XXXXXX	.XXXXXX	.XXXXXX	.XXXXXX	.XXXXXX	.XXXXXX	.XXXXXX	.XXXXXX	.XXXXXX	.XXXXXX	.XXXXXX
XXX.XXXX	XXX.XXXX	XX.XXXX	XX.XXXX	XX.XXXX	XX.XXXX	XX.XXXX	XX.XXXX	XX.XXXX	XX.XXXX	XX.XXXX	XX.XXXX
.XXXXXX	.XXXXXX	.XXXXXX	.XXXXXX	.XXXXXX	.XXXXXX	.XXXXXX	.XXXXXX	.XXXXXX	.XXXXXX	.XXXXXX	.XXXXXX
XXX.XXXX	XXX.XXXX	XX.XXXX	XX.XXXX	XX.XXXX	XX.XXXX	XX.XXXX	XX.XXXX	XX.XXXX	XX.XXXX	XX.XXXX	XX.XXXX
.XXXXXX	.XXXXXX	.XXXXXX	.XXXXXX	.XXXXXX	.XXXXXX	.XXXXXX	.XXXXXX	.XXXXXX	.XXXXXX	.XXXXXX	.XXXXXX
XXX.XXXX	XXX.XXXX	XX.XXXX	XX.XXXX	XX.XXXX	XX.XXXX	XX.XXXX	XX.XXXX	XX.XXXX	XX.XXXX	XX.XXXX	XX.XXXX
.XXXXXX	.XXXXXX	.XXXXXX	.XXXXXX	.XXXXXX	.XXXXXX	.XXXXXX	.XXXXXX	.XXXXXX	.XXXXXX	.XXXXXX	.XXXXXX

elastic bending characteristics of the torque tube and the inboard (snubber) end vertical deflection of the torque tube. For each, a quadratic variation with pitch angle is assumed so that the total bending stiffness matrix, FDEFL, and inboard deflection vector, Z5I, are formed in the indicated manner wherein the total blade pitch angle at the 75 percent span, TTHO, is taken in radians. Furthermore, all the results output for these two quantities are nondimensional (see the superscripts section of the List of Symbols for the proper nondimensionalization). The matrix FDEFL duplicates matrix S, whose rows and columns are defined by equation (108) of Reference 1; vector Z5I shares the same columnar dependence with matrix FDEFL. Finally, at the bottom of Sample Page 3 are evaluations of FDEFL and Z5I, using the quadratic representations, at a pitch angle equal to the inputted collective angle, $0.75R$. It should be noted that the functionalizations of these quantities to quadratic form is accomplished by matching exactly the quantities calculated with pitch angles equal to the collective angles.

The first group of output parameters given in Sample Page 4 consists of the (nondimensional) coefficients defining the nonlinear torsional stiffness characteristics of the flexbeam; they correspond directly to the coefficients defined in Reference 1. Again the standard nondimensionalization is used. The second group of output parameters on the sample page consists of the quadratic functionality coefficients for the pitch-flat and pitch-edge couplings and the angular motions of the torque tube relative to the flexbeam at the juncture for each of the selected flatwise and edgewise modes. The quadratic functionality on pitch angle duplicates that used for FDEFL and Z5I described in the above paragraph. Note that RELMW and RELMV are calculated only on the basis of an infinitely rigid torque tube and, hence, are omitted when the redundant analysis option is invoked. The third group of output parameters are the effective torsional springs $K_{\theta 1}$, $K_{\theta 2}$, and $K_{\theta 3}$, as defined in Reference 1, and the flexbeam stiffness, GJ and Tk_a , respectively. The units of the springs are lb-ft/rad and those of the stiffnesses are lb-ft².

In Sample Page 5 are shown typical modal information for the inputted flatwise and edgewise bending modes. For each such mode the (nondimensional) modal frequency, pitch-flat (or pitch-edge) coupling and inputted mode shape and spanwise derivatives are listed. In addition the listing presents the derived incremental deflection vectors which account for blade twist (see equations (7-10), of Reference 1. Within a flatwise modal information group, the DVB and DVE arrays correspond to those first order Δv spanwise functions due to built-in twist and torsional modal twist, respectively. The DWWBB, DWWBC and DWWCC arrays correspond to those second order ΔW functions due to the combinations of built-in twist with itself, built-in twist with pseudo-torsion mode (control) twist, and pseudo-torsion mode twist with itself, respectively. The various arrays, DV2BP, DV2EP, DWW2BBP, DWW2BCP and DWW2CCP are the first spanwise derivatives of the second components (those with superscript "2") of the above discussed arrays, DVB, DVE, DWWBB, DWWBC, and DWWCC, respectively.

[illegible][illegible][illegible]

030 XXXX = 52-V13M1 = CH11

[illegible]

Sample Page 3

FLEX-BEAM TORSIONAL STIFFNESS CHARACTERISTICS

$$\begin{aligned} \text{THETA-JCT} = & (\text{THTHP}) * \text{THETAP-JCT} + (\text{THTMX}) * \text{MX5} + (\text{THTSX}) * \text{SX5} * (\text{Y5} * \text{Z5}' - \text{Z5} * \text{Y5}') \\ & + (\text{THTMO}) * (\text{MY5} * \text{Y5} + \text{MZ5} * \text{Z5}) + (\text{THTM1}) * (\text{MY5} * \text{Y5}' + \text{MZ5} * \text{Y5}') + (\text{THTSO}) * (\text{SZ5} * \text{Y5} - \text{SY5} * \text{Z5}) \\ & + (\text{THTS1}) * (\text{SZ5} * \text{Y5}' - \text{SY5} * \text{Z5}') \end{aligned}$$

THTHP	THTMX	THTSX	THTMO	THTM1	THTSO	THTS1
XXX.XXXXXX	XXX.XXXXXX	XXX.XXXXXX	XXX.XXXXXX	XXX.XXXXXX	XXX.XXXXXX	XXX.XXXXXX

COEFFICIENTS FOR QUADRATIC VARIATIONS OF PITCH-FLAT AND PITCH-EDGE COUPLINGS WITH PITCH ANGLE

I	A ₀ (I)	A ₁ (I)	A ₂ (I)	REL ^W (I)
1	.XXXXX	.XXXXX	.XXXXX	.XXXXX
2	.XXXXX	.XXXXX	.XXXXX	.XXXXX
3	.XXXXX	.XXXXX	.XXXXX	.XXXXX

K	AV ₀ (K)	AV ₁ (K)	AV ₂ (K)	REL ^V (K)
1	.XXXXX	.XXXXX	.XXXXX	.XXXXX
2	.XXXXX	.XXXXX	.XXXXX	.XXXXX

TORSIONAL RETENTION SPRINGS AND EFFECTIVE FLEX-BEAM TORSIONAL STIFFNESSES

KTHETA1	KTHETA2	KTHETA3	GJ-EFF	TKA2
XXX.XXXXX	XXX.XXXXX	XXX.XXXXX	XXX.XXXXX	XXX.XXXXX

LINEAR AND NONLINEAR MODAL DEFLECTION VECTORS

FLATWISE MODE 1		MODAL FREQUENCY = X.XXXXX					PITCH-FLAT COUPLING, AM(1) = .XXXXX					
N	X	GM	GMP	GWPP	DVB	DV2BP	DWMBB	DW2BBP	DWBC	DW2BCP	DWCC	DW2CCP
1	.XXXXX	.XXXXX	.XXXXX	.XXXXX	.XXXXX	.XXXXX	.XXXXX	.XXXXX	.XXXXX	.XXXXX	.XXXXX	.XXXXX
2	.XXXXX	.XXXXX	.XXXXX	.XXXXX	.XXXXX	.XXXXX	.XXXXX	.XXXXX	.XXXXX	.XXXXX	.XXXXX	.XXXXX
3	.XXXXX	.XXXXX	.XXXXX	.XXXXX	.XXXXX	.XXXXX	.XXXXX	.XXXXX	.XXXXX	.XXXXX	.XXXXX	.XXXXX
.	.XXXXX	.XXXXX	.XXXXX	.XXXXX	.XXXXX	.XXXXX	.XXXXX	.XXXXX	.XXXXX	.XXXXX	.XXXXX	.XXXXX
.	.XXXXX	.XXXXX	.XXXXX	.XXXXX	.XXXXX	.XXXXX	.XXXXX	.XXXXX	.XXXXX	.XXXXX	.XXXXX	.XXXXX
.	.XXXXX	.XXXXX	.XXXXX	.XXXXX	.XXXXX	.XXXXX	.XXXXX	.XXXXX	.XXXXX	.XXXXX	.XXXXX	.XXXXX
.	.XXXXX	.XXXXX	.XXXXX	.XXXXX	.XXXXX	.XXXXX	.XXXXX	.XXXXX	.XXXXX	.XXXXX	.XXXXX	.XXXXX
4	.XXXXX	.XXXXX	.XXXXX	.XXXXX	.XXXXX	.XXXXX	.XXXXX	.XXXXX	.XXXXX	.XXXXX	.XXXXX	.XXXXX

QUADRATIC DEFLECTION VECTORS DUE TO TORSION MODAL TWIST (DVE(1,J), DV2EP(1,J)), AND TO FLATWISE BENDING, UVE(1,M)

		J = (1)		(2)		(3)		/ M = (1)		(2)	(3)	(4)
N	X	DVE	DV2EP	DVE	DV2EP	DVE	DV2EP	/		UVE		
1	.XXXXX	.XXXXX	.XXXXX	.XXXXX	.XXXXX	.XXXXX	.XXXXX	.XXXXX	.XXXXX	.XXXXX	.XXXXX	.XXXXX
2	.XXXXX	.XXXXX	.XXXXX	.XXXXX	.XXXXX	.XXXXX	.XXXXX	.XXXXX	.XXXXX	.XXXXX	.XXXXX	.XXXXX
3	.XXXXX	.XXXXX	.XXXXX	.XXXXX	.XXXXX	.XXXXX	.XXXXX	.XXXXX	.XXXXX	.XXXXX	.XXXXX	.XXXXX
.	.XXXXX	.XXXXX	.XXXXX	.XXXXX	.XXXXX	.XXXXX	.XXXXX	.XXXXX	.XXXXX	.XXXXX	.XXXXX	.XXXXX
.	.XXXXX	.XXXXX	.XXXXX	.XXXXX	.XXXXX	.XXXXX	.XXXXX	.XXXXX	.XXXXX	.XXXXX	.XXXXX	.XXXXX
.	.XXXXX	.XXXXX	.XXXXX	.XXXXX	.XXXXX	.XXXXX	.XXXXX	.XXXXX	.XXXXX	.XXXXX	.XXXXX	.XXXXX
.	.XXXXX	.XXXXX	.XXXXX	.XXXXX	.XXXXX	.XXXXX	.XXXXX	.XXXXX	.XXXXX	.XXXXX	.XXXXX	.XXXXX
4	.XXXXX	.XXXXX	.XXXXX	.XXXXX	.XXXXX	.XXXXX	.XXXXX	.XXXXX	.XXXXX	.XXXXX	.XXXXX	.XXXXX

EDGEWISE MODE 1		MODAL FREQUENCY = X.XXXXX					PITCH-EDGE COUPLING, AV(1) = .XXXXX					
N	X	GV	GVP	GWPP	DVB	DV2BP	DVMBB	DV2BBP	DVBC	DV2BCP	DVCC	DV2CCP
1	.XXXXX	.XXXXX	.XXXXX	.XXXXX	.XXXXX	.XXXXX	.XXXXX	.XXXXX	.XXXXX	.XXXXX	.XXXXX	.XXXXX
2	.XXXXX	.XXXXX	.XXXXX	.XXXXX	.XXXXX	.XXXXX	.XXXXX	.XXXXX	.XXXXX	.XXXXX	.XXXXX	.XXXXX
3	.XXXXX	.XXXXX	.XXXXX	.XXXXX	.XXXXX	.XXXXX	.XXXXX	.XXXXX	.XXXXX	.XXXXX	.XXXXX	.XXXXX
.	.XXXXX	.XXXXX	.XXXXX	.XXXXX	.XXXXX	.XXXXX	.XXXXX	.XXXXX	.XXXXX	.XXXXX	.XXXXX	.XXXXX
.	.XXXXX	.XXXXX	.XXXXX	.XXXXX	.XXXXX	.XXXXX	.XXXXX	.XXXXX	.XXXXX	.XXXXX	.XXXXX	.XXXXX
.	.XXXXX	.XXXXX	.XXXXX	.XXXXX	.XXXXX	.XXXXX	.XXXXX	.XXXXX	.XXXXX	.XXXXX	.XXXXX	.XXXXX
.	.XXXXX	.XXXXX	.XXXXX	.XXXXX	.XXXXX	.XXXXX	.XXXXX	.XXXXX	.XXXXX	.XXXXX	.XXXXX	.XXXXX
4	.XXXXX	.XXXXX	.XXXXX	.XXXXX	.XXXXX	.XXXXX	.XXXXX	.XXXXX	.XXXXX	.XXXXX	.XXXXX	.XXXXX

DEFLECTION VECTORS DUE TO ELASTIC (MODAL) TWIST, DVE(1,J), DV2EP(1,J), AND TO EDGEWISE BENDING, UVE(1,M)

		J = (1)		(2)		(3)				UVE		
N	X	DVE	DV2EP	DVE	DV2EP	DVE	DV2EP					
1	.XXXXX	.XXXXX	.XXXXX	.XXXXX	.XXXXX	.XXXXX	.XXXXX	.XXXXX	.XXXXX	.XXXXX	.XXXXX	.XXXXX
2	.XXXXX	.XXXXX	.XXXXX	.XXXXX	.XXXXX	.XXXXX	.XXXXX	.XXXXX	.XXXXX	.XXXXX	.XXXXX	.XXXXX
3	.XXXXX	.XXXXX	.XXXXX	.XXXXX	.XXXXX	.XXXXX	.XXXXX	.XXXXX	.XXXXX	.XXXXX	.XXXXX	.XXXXX
.	.XXXXX	.XXXXX	.XXXXX	.XXXXX	.XXXXX	.XXXXX	.XXXXX	.XXXXX	.XXXXX	.XXXXX	.XXXXX	.XXXXX
.	.XXXXX	.XXXXX	.XXXXX	.XXXXX	.XXXXX	.XXXXX	.XXXXX	.XXXXX	.XXXXX	.XXXXX	.XXXXX	.XXXXX
.	.XXXXX	.XXXXX	.XXXXX	.XXXXX	.XXXXX	.XXXXX	.XXXXX	.XXXXX	.XXXXX	.XXXXX	.XXXXX	.XXXXX
.	.XXXXX	.XXXXX	.XXXXX	.XXXXX	.XXXXX	.XXXXX	.XXXXX	.XXXXX	.XXXXX	.XXXXX	.XXXXX	.XXXXX
4	.XXXXX	.XXXXX	.XXXXX	.XXXXX	.XXXXX	.XXXXX	.XXXXX	.XXXXX	.XXXXX	.XXXXX	.XXXXX	.XXXXX

The UWE nonlinear deflection arrays correspond to the bracketed integral function defined in Reference 1. Within the edgewise modal information group, the various arrays, DWB, DWE, DVBB, DVVBC and DVVCC, etc., correspond to similarly defined spanwise functions involving twist and the edgewise modal deflection and spanwise derivative arrays.

The output parameters presented in Sample Page 6 consist of the inputted torsion modal arrays together with the derived pseudo-torsion mode shape (as defined in Reference 1) and spanwise derivative. The output parameter group presented in Sample Page 7 consists of the spanwise distributions of various pertinent aeroelastic quantities. The X and XCEN arrays are the nondimensional distances of the centers of the segments from the offset and rotor axis, respectively. The units of the CHORD array are feet. The angle of attack descriptors THETA-AERO, PHI and ALPHA are, respectively, the geometric aerodynamic pitch angle, the inflow angle, and the resulting section angle-of-attack, all in degrees. These angles are calculated using the input initial conditions on azimuth angle and on the response variable deflections and velocities. The resulting Mach number and aerodynamic coefficients are used to define the perturbational airloads used in the eigensolution. The quantity KAPPA/U is the spanwise variation in aerodynamic moment damping coefficient which when multiplied by the local pitch rate approximates the potential flow unsteady pitching moment coefficient. The quantity (Y10C/4)/C is the spanwise distribution of quarter chord offset from the reference axis nondimensionalized by chord. The dynamic and structural quantities in the third group of this output page includes the QUAD array which constitutes the integration weighting numbers for spanwise integration. The THETA-STR array is the pitch angle distribution of the structural principle axes and has the units of degrees and, in general, differs from the aerodynamic pitch angle distribution. The two arrays, TWIST-BLT and TWIST-TOT, are the nondimensional structural twist rate distributions of the built-in twist and the total twist (including elastic response and control inputs), respectively; these arrays have the units of radians. The quantities TENSB, EIYB, EIZB, and MASSB are, respectively, the blade tension, flatwise bending stiffness, edgewise bending stiffness and mass distributions, all nondimensionalized in the standard sense. The (Y10NA)/C and (Y10CG)/C arrays are, respectively, the edgewise bending neutral axis and mass center offset distributions nondimensionalized by chord.

Results of Time History Solutions

Sample Page 8 presents a variety of response and load quantities defining the transient aeroelastic responses. The first row of parameters following the page title presents, for the time-history solution, a listing of the parameters defining the flight condition. These parameters consist of the various control angles (in degrees), the inflow and advance ratios, and the nondimensionalized values of the "momentum" induced velocity components. The remainder

TORSION MODES

MODAL FREQ(1) = X.XXXXX MODAL FREQ(2) = X.XXXXX MODAL FREQ(3) = X.XXXXX

N	X	GT(1)	GTP(1)	GT(2)	GTP(2)	GT(3)	GTP(3)
1	.XXXXX	.XXXXX	.XXXXX	.XXXXX	.XXXXX	.XXXXX	.XXXXX
2	.XXXXX	.XXXXX	.XXXXX	.XXXXX	.XXXXX	.XXXXX	.XXXXX
3	.XXXXX	.XXXXX	.XXXXX	.XXXXX	.XXXXX	.XXXXX	.XXXXX
.	.XXXXX	.XXXXX	.XXXXX	.XXXXX	.XXXXX	.XXXXX	.XXXXX
.	.XXXXX	.XXXXX	.XXXXX	.XXXXX	.XXXXX	.XXXXX	.XXXXX
.	.XXXXX	.XXXXX	.XXXXX	.XXXXX	.XXXXX	.XXXXX	.XXXXX
.	.XXXXX	.XXXXX	.XXXXX	.XXXXX	.XXXXX	.XXXXX	.XXXXX
N	.XXXXX	.XXXXX	.XXXXX	.XXXXX	.XXXXX	.XXXXX	.XXXXX

Sample Page 6

PIPIAL DISTRIBUTIONS OF AERODYNAMIC AND DYNAMIC/STRUCTURAL QUANTITIES

N	X	XCEN	CHORD	THETA-AERO	PHI	ALPHA	MACH	CL	CD	CM	KAPPA/U	(Y10C/4)/C
1	.XXXXX	.XXXXX	.XXXXX	A.XXX	.XXX	X.XXX	.XXX	.XXXXX	.XXXXX	.XXXXX	.XXXXX	.XXXXX
2	.XXXXX	.XXXXX	.XXXXX	X.XXX	.XXX	X.XXX	.XXX	.XXXXX	.XXXXX	.XXXXX	.XXXXX	.XXXXX
3	.XXXXX	.XXXXX	.XXXXX	X.XXX	.XXX	X.XXX	.XXX	.XXXXX	.XXXXX	.XXXXX	.XXXXX	.XXXXX
.	.XXXXX	.XXXXX	.XXXXX	X.XXX	.XXX	X.XXX	.XXX	.XXXXX	.XXXXX	.XXXXX	.XXXXX	.XXXXX
.	.XXXXX	.XXXXX	.XXXXX	X.XXX	.XXX	X.XXX	.XXX	.XXXXX	.XXXXX	.XXXXX	.XXXXX	.XXXXX
.	.XXXXX	.XXXXX	.XXXXX	X.XXX	.XXX	X.XXX	.XXX	.XXXXX	.XXXXX	.XXXXX	.XXXXX	.XXXXX
N	.XXXXX	.XXXXX	.XXXXX	X.XXX	.XXX	X.XXX	.XXX	.XXXXX	.XXXXX	.XXXXX	.XXXXX	.XXXXX

N	X	XCEN	QUAD	THETA-STR	TWIST-BLT	TWIST-TOT	TENSB	E1Y5	E1Y6	(Y10N4)/C	MAS5B	(Y10C6)/C
1	.XXXXX	.XXXXX	.XXXXX	X.XXX	.XXXXX	.XXXXX	.XXXXX	.XXXXX	.XXXXX	.XXXXX	X.XXXXX	.XXXXX
2	.XXXXX	.XXXXX	.XXXXX	X.XXX	.XXXXX	.XXXXX	.XXXXX	.XXXXX	.XXXXX	.XXXXX	X.XXXXX	.XXXXX
3	.XXXXX	.XXXXX	.XXXXX	X.XXX	.XXXXX	.XXXXX	.XXXXX	.XXXXX	.XXXXX	.XXXXX	X.XXXXX	.XXXXX
.	.XXXXX	.XXXXX	.XXXXX	X.XXX	.XXXXX	.XXXXX	.XXXXX	.XXXXX	.XXXXX	.XXXXX	X.XXXXX	.XXXXX
.	.XXXXX	.XXXXX	.XXXXX	X.XXX	.XXXXX	.XXXXX	.XXXXX	.XXXXX	.XXXXX	.XXXXX	X.XXXXX	.XXXXX
.	.XXXXX	.XXXXX	.XXXXX	X.XXX	.XXXXX	.XXXXX	.XXXXX	.XXXXX	.XXXXX	.XXXXX	X.XXXXX	.XXXXX
N	.XXXXX	.XXXXX	.XXXXX	X.XXX	.XXXXX	.XXXXX	.XXXXX	.XXXXX	.XXXXX	.XXXXX	X.XXXXX	.XXXXX

Sample Page 7

PART II. TIME HISTORY SOLUTION OF COMPLETE (NONLINEAR) EQUATION SET - AEROELASTIC TRANSIENT RESPONSES

	A15	B15	A25	B25	THETA 75	LAM9DA	MU	VO	VIC	VIS
	X.XXX	X.XXX	X.XXX	X.XXX	X.XXX	X.XXX	X.XXX	X.XXX	X.XXX	X.XXX

PSI = X.XX DEG. OFV = XX

N	X CLN	PMI	ALPHA	MACH NO.	CL	CU	CM	SAZ5	SAVS	MALE	SDZ5	SDVS	MDZ5	MEV9
1	.XXXX	X.XXX	X.XXX	.XXX	V.XXXX	.XXXX	V.XXXX	.XXXX	.XXXX	.XXXX	.XXXX	.XXXX	.XXXX	.XXXX
2	.XXXX	X.XXX	X.XXX	.XXX	V.XXXX	.XXXX	V.XXXX	.XXXX	.XXXX	.XXXX	.XXXX	.XXXX	.XXXX	.XXXX
3	.XXXX	X.XXX	X.XXX	.XXX	V.XXXX	.XXXX	V.XXXX	.XXXX	.XXXX	.XXXX	.XXXX	.XXXX	.XXXX	.XXXX
.	.XXXX	X.XXX	X.XXX	.XXX	V.XXXX	.XXXX	V.XXXX	.XXXX	.XXXX	.XXXX	.XXXX	.XXXX	.XXXX	.XXXX
.	.XXXX	X.XXX	X.XXX	.XXX	V.XXXX	.XXXX	V.XXXX	.XXXX	.XXXX	.XXXX	.XXXX	.XXXX	.XXXX	.XXXX
.	.XXXX	X.XXX	X.XXX	.XXX	V.XXXX	.XXXX	V.XXXX	.XXXX	.XXXX	.XXXX	.XXXX	.XXXX	.XXXX	.XXXX
.	.XXXX	X.XXX	X.XXX	.XXX	V.XXXX	.XXXX	V.XXXX	.XXXX	.XXXX	.XXXX	.XXXX	.XXXX	.XXXX	.XXXX
4	.XXXX	X.XXX	X.XXX	.XXX	V.XXXX	.XXXX	V.XXXX	.XXXX	.XXXX	.XXXX	.XXXX	.XXXX	.XXXX	.XXXX

	C61	C62	C63	C64	OV1	OV2	OV3	OT1	OT2	OT3	BETA	DELTA	BETA-P1	BETA-P2
X1	X.XXX-VV	X.XXX-VV	X.XXX-VV	X.XXX-VV	X.XXX-VV	X.XXX-VV	X.XXX-VV	X.XXX-VV	X.XXX-VV	X.XXX-VV	X.XXX-VV	X.XXX-VV	X.XXX-VV	X.XXX-VV
000	X.XXX-VV	X.XXX-VV	X.XXX-VV	X.XXX-VV	X.XXX-VV	X.XXX-VV	X.XXX-VV	X.XXX-VV	X.XXX-VV	X.XXX-VV	X.XXX-VV	X.XXX-VV	X.XXX-VV	X.XXX-VV
C6	X.XXX-VV	X.XXX-VV	X.XXX-VV	X.XXX-VV	X.XXX-VV	X.XXX-VV	X.XXX-VV	X.XXX-VV	X.XXX-VV	X.XXX-VV	X.XXX-VV	X.XXX-VV	X.XXX-VV	X.XXX-VV
0	X.XXX-VV	X.XXX-VV	X.XXX-VV	X.XXX-VV	X.XXX-VV	X.XXX-VV	X.XXX-VV	X.XXX-VV	X.XXX-VV	X.XXX-VV	X.XXX-VV	X.XXX-VV	X.XXX-VV	X.XXX-VV

N	CEN	VERTICAL DEFL-IN	INPLANE DEFL-IN	TORSION DEFL-DEG	FLATWISE STRESS	EDGEWISE STRESS	TORSION STRESS	CORNER STRESS	TORSION MOMENT	A	9
1	.XXXX	.XXX	.XXX	.XXX	.XXXX	.XXXX	.XXXX	.XXXX	.XXXX	.XXXX	.XXXX
2	.XXXX	.XXX	.XXX	.XXX	.XXXX	.XXXX	.XXXX	.XXXX	.XXXX	.XXXX	.XXXX
3	.XXXX	.XXX	.XXX	.XXX	.XXXX	.XXXX	.XXXX	.XXXX	.XXXX	.XXXX	.XXXX
.	.XXXX	.XXX	.XXX	.XXX	.XXXX	.XXXX	.XXXX	.XXXX	.XXXX	.XXXX	.XXXX
.	.XXXX	.XXX	.XXX	.XXX	.XXXX	.XXXX	.XXXX	.XXXX	.XXXX	.XXXX	.XXXX
.	.XXXX	.XXX	.XXX	.XXX	.XXXX	.XXXX	.XXXX	.XXXX	.XXXX	.XXXX	.XXXX
4	.XXXX	.XXX	.XXX	.XXX	.XXXX	.XXXX	.XXXX	.XXXX	.XXXX	.XXXX	.XXXX

SPAR/FLEXURE PARAMETERS:

2	.XXXX	XXXX.	XXX.	XXXX.	XXXX.	XXX.XX
PUSH-ROD (RELATIVE) DEFL. =	.XX IN					PUSH-ROD LOAD = XXX.XX LB
TORQUE-TUBE ROOT DEFL. =	.XX IN					TORQUE-TUBE ROOT SHEAR = XXX.XX LB

of Sample Page 8 comprises the typical azimuthal listing; this listing is outputted for every azimuth angle which is a multiple of the print azimuth increment, input item no. 23.

The first of the four groups of result quantities on this sample page lists the spanwise distributions of the pertinent aerodynamic quantities. The inflow and total section angles of attack PHI and ALPHA, respectively, are in degrees. The MACH NO., CL, CD, and CM are self-explanatory and nondimensional. The airload distributions in the Z5 and Y5 directions, SAZ5 and SAY5, respectively, have the units of lb/in., the aerodynamic pitching moment distribution, MAX5, has the units of in.-lb/in. The quantities SDZ5, SDY5 and MDX5 are "semi-dynamic" load distributions. These distributions are dimensionally similar to those above described resulting from aerodynamics, but instead arise from all the dynamic effects except those involving second time differentiations of the response variables (i.e., q_{w1}^{**} , q_{vk}^{**} , etc.). The quantity MEX9 is the elastic torsion moment distribution which consists of those torsion couplings arising from ΔEI , the tension-neutral axis offset and other twist related elastic effects; it too, has the units of in.-lb/in.

The second group of result quantities consists of the instantaneous generalized excitations, XI, and the generalized accelerations, velocities, and displacements (Q^{**} , Q^* , and Q , respectively), for each of the modal response variables selected, all appropriately nondimensionalized. The generalized excitations are defined to be the elements of the right hand sides of the dynamic equations.

The third group of result quantities are comprised mainly of blade deflection and stress distributions. The vertical and inplane deflections are those in the Z5 and Y5 directions, respectively. All stress quantities have the units of lb/in.², whereas the torsion moment has the units of lb-in. It should be noted that, over the flexbeam-torque tube span, the flatwise and edgewise stresses outputted are those only for the flexbeam whereas the torsion moments and stresses outputted are those only for the torque tube. The last two columns are the distributions of the A and B parameters needed to define the unsteady airloads. The fourth group of result quantities at the bottom of the sample page consists of miscellaneous deflection, load and stress results for the flexbeam and push-rod.

The line titled SPAR/FLEXURE PARAMETERS presents similar stresses and torsion moments for the flexbeam at the indicated spanwise location; note, however, that the output torsion moment is for the flexbeam immediately inboard of the juncture. Of the remaining four quantities, PUSH-ROD (RELATIVE) DEFL. (in.), TORQUE TUBE ROOT DEFL. (in.), and TORQUE TUBE ROOT SHEAR (lb) pertain only to cantilevered torque tube configurations wherein the "wobble mode" option is invoked (input location 985). All three quantities are defined in the positive Z5 direction. The quantity PUSH-ROD LOAD (lb)

is the upward (+Z5) directed load the push-rod exerts on the pitch horn/push-rod attachment point; this quantity is calculated for all blade types. For composite bearingless rotors, the push-rod load accounts for the total blade torsion moment at the root less that torsion moment resisted by the flexbeam.

After the time-history solution has either converged to periodicity or run to maximum flapping trials (input location 10) various integrated loads are calculated for one final blade revolution to form the aerodynamic performance and stress results depicted in Sample Page 9. For each of eight (8) performance quantities results are presented in nondimensional coefficient form, in nondimensional form divided by solidity, and in actual dimensional form. Note that ten (10) dimensional quantities are listed and the units are lb for forces and lb-ft for moments, as appropriate. The quantity EQU. DRAG (1b) represents the combined power expended by the rotor due to rotor rotation (torque) and translation (drag) divided by flight speed.

The next line duplicates the parameters defining the flight condition and includes four (4) additional quantities which depend on the integrated performance for evaluation. At the beginning of the time-history calculation it is not known which part of the inflow ratio being used is due to ram effects and which due to momentum induced effects. Once the integrated rotor thrust is calculated, however, the induced portion of the inflow can then be calculated using the simple usual momentum formula derived for flight in an infinite continuum. The complementary portion of the inflow represents the ram effect from which the shaft angle-of-attack ALPHA S, in degrees, can be calculated. The quantity VEL ACT. is the actual forward flight velocity, in knots, consistent with the advance ratio used and the shaft angle of attack. For finite forward flight speeds EQU. L/D is the lift divided by the equivalent drag; for hovering cases this quantity is the figure of merit. PAR. AREA, the rotor parasite (drag) area, in square feet, is the rotor drag divided by dynamic pressure. The line titled CORRECTIONS DUE TO WIND TUNNEL WALL INTERFERENCE: consists of recalculations of those quantities which depend on the induced portion of the inflow wherein the induced inflow is calculated using the formulae derived for flight in wind tunnels or in ground effect. The remainder of Sample Page 9 consists of reductions of the various stresses (lb/in.²) and the push-rod load (lb) to median and 1/2 peak-to-peak values over the final rotor revolution.

Should major (trim) iterations be used (see descriptions of input items 60 and 62 through 65) two similar types of page output will be generated. The trim calculation first calculates a trim matrix of partial derivatives. For this calculation the blade pitch control angles (or, optionally, components of Glauert inflow) and shaft angle are systematically incremented to form the numerical partial derivatives. During the calculation of these partial derivatives, the time history solution is run separately five times to

PUSH-HOLD LEAD (MEDIAN, 1/7 PIP):

[illegible]

ALPHA 5 = XXXX 060. LIST = XXXX,XX LB PF = XXX,XX LB WFL ACT. = XXX,XX NT.

:JCN3833631MI 774# 7J4N01 04I# 01 JND S4UJ1J38R0C

[illegible]

ACCOYDYNAMIC PERFORMANCE AND STRESSES

establish the base values and the four perturbations. An output page is generated for each of these five runs. Each of these pages has the combined form of the first three lines of Sample Page 8 (giving header information) and the aerodynamic portion of Sample Page 9 (exclusive of the stress results).

Once the partial derivative matrix has been calculated from the perturbational calculations, the second type of trim related page output is generated, and is shown in Sample Page 10. This page, which is repeated for each trim iteration, consists of the same output as is generated while incrementing the control quantities (as discussed above) together with additional specific trim iterative information. The first line of this additional information consists of the iteration number, the zeroth, first cosine and first and second sine harmonics of first flatwise mode response, in radians, and an estimate of an effective angle-of-attack on the retreating blade side ($\psi = 270^\circ$), in degrees. The nonzero elements of the TRIM PARTIAL DERIVATIVE MATRIX give, for each row, the partial derivatives of the four trim quantities (C_L , C_{PF} , C_{PM} , C_{RM} , respectively) with respect to the four control quantities being used ($\theta_{.75}$, A_{1s} , B_{1s} , and $(\sin \alpha_s)$, or v_o , v_{1c} , v_{1s} , and $(\sin \alpha_s)$), for each respective column. The elements of this matrix are formulated using approximate linear strip theory (with reversed flow effects) or numerical differentiation and are calculated for either set of control quantities. The ERROR VECTOR consists of the differences between the four requested trim quantities and those achieved in the preceeding time-history. The two lines depicted give the error vector in dimensional (lb and lb-ft) and nondimensional forms, respectively. The TRIM VARIABLE CORRECTION VECTOR consists of those changes to the control quantities which should null the above described error vector. The correction vector is obtained from the premultiplication of the inverse of the G matrix with the error vector, but the corrections are scaled, if necessary, to prevent control changes of more than 2 degrees within any one iteration. The control parameters whose increments are depicted in this output page are, in respective order: $\theta_{.75}$, A_{1s} , B_{1s} , $(\sin \alpha_s)$, λ , C_T , v_o , v_{1c} , and v_{1s} ; the first three have units of degrees and the remainder are dimensionless or nondimensionalized.

PART II. TIME HISTORY SOLUTION OF COMPLETE (NONLINEAR) EQUATION SET - AEROELASTIC TRANSIENT RESPONSES

A1S	B1S	A2S	B2S	THETA 75	LAMBDA	MU	VO	V1C	V1S
X.XXX	X.XXX	X.XXX	X.XXX	X.XXX	.XXXXX	.XXX	.XXXXX	.XXXXX	.XXXXX

AERODYNAMIC PERFORMANCE AND STRESSES

	H FORCE	Y FORCE	THRUST	ROLL. MOM.	PITCH MOM.	TORQUE	LIFT	PROP. FORCE	HORSEPOWER	EQU. DRAG
C()	.XXXXXXXX	.XXXXXXXX	.XXXXXXXX	.XXXXXXXX	.XXXXXXXX	.XXXXXXXX	.XXXXXXXX	.XXXXXXXX		
C()/SIG	.XXXXXXXX	.XXXXXXXX	.XXXXXXXX	.XXXXXXXX	.XXXXXXXX	.XXXXXXXX	.XXXXXXXX	.XXXXXXXX		
DIMENS.	XX.XX	XX.XX	XX.XX	XX.XX	XX.XX	XX.XX	XX.XX	XX.XX	XX.XX	XX.XX

A1S	B1S	A2S	B2S	THETA 75	LAMBDA	MU	VEL ACT.	EQU. L/D	PAR. AREA	ALPHA S
.XXX	.XXX	.XXX	.XXX	.XXX	.XXXXX	.XXX	XX.XX	.XXX	.XXX	.XXX

TRIM ITERATION NO. 99, QW10 = X.XXE-YY QW1C = X.XXE-YY QW1S = X.XXE-YY QW2S = X.XXE-YY A(270) = XX.XX

TRIM PARTIAL DERIVATIVE MATRIX, D(CL,CPF,CPM,CRM)/D(XX(1),SIN(ALPHAS)) (XX(1)= TH75 OR VO, XX(2)= A1S OR V1C, XX(3)= B1S OR V1S

X.XXXE-YY	X.XXXE-YY	X.XXXE-YY	X.XXXE-YY
X.XXXE-YY	X.XXXE-YY	X.XXXE-YY	X.XXXE-YY
X.XXXE-YY	X.XXXE-YY	X.XXXE-YY	X.XXXE-YY
X.XXXE-YY	X.XXXE-YY	X.XXXE-YY	X.XXXE-YY

ERROR VECTOR (DIMENSIONAL AND NONDIMENSIONAL)

X.XXXE-YY	X.XXXE-YY	X.XXXE-YY	X.XXXE-YY
X.XXXE-YY	X.XXXE-YY	X.XXXE-YY	X.XXXE-YY

TRIM VARIABLE CORRECTION VECTOR, DXX(1) (1= TH75, 2= A1S, 3= B1S, 4= SIN(ALPHAS), 5= LAMBDA, 6= VO, 7= V1C, 8= V1S)

X.XXXE-YY	X.XXXE-YY	X.XXXE-YY	X.XXXE-YY	X.XXXE-YY	X.XXXE-YY	X.XXXE-YY	X.XXXE-YY
-----------	-----------	-----------	-----------	-----------	-----------	-----------	-----------

Once the time-history solution has converged to periodicity and all major iterations have been completed, the program optionally performs harmonic analyses of the azimuthal variations of various response quantities (see descriptions of input items 48 and 73 through 75). The outputs of these harmonic analyses are depicted in Sample Pages 11 through 13. In each of these sample pages the harmonic information for each response variable is contained in the appropriate horizontal band of five rows. The harmonics are listed by columns up to a maximum of 10 harmonics. All harmonic analysis output depicted on these sample pages assume a negative harmonic content form in keeping with the (negative) harmonic form conventionally assumed for the blade pitch control and rigid flapping angles. For each harmonic of response variable five quantities are outputted; these quantities are, respectively, the cosine and sine components, the equivalent amplitude and phase angle, and lastly, the amplitude of the harmonic relative to all the other harmonic amplitudes outputted. Sample Page 11 depicts the harmonic analyses of the dimensionless modal response variables selected wherein QW(I), QV(K), and QT(J) are, respectively, the (I) flatwise, (K) edgewise and (J) torsional uncoupled mode responses.

Sample Page 12 depicts the harmonic analyses of the total shears and moments exerted by one blade to the hub. In contrast to the steady hub loads listed in the AERODYNAMIC PERFORMANCE AND STRESSES output (Sample Page 9) which are calculated by integrating only the aerodynamic load distributions, the total hub loads which are herein harmonically analyzed are calculated by similarly integrating the combined aerodynamic and the dynamic load distributions. The longitudinal, lateral and vertical hub shears comprising the first three quantities of this sample page all have the dimensions of lb and are defined in the x_1 -(aft), y_1 -(starboard), and z_1 -(up and along axis of rotation) axis directions, respectively. The roll, pitch and yaw moments comprising the latter three quantities on this sample page have the dimensions of lb-ft and are defined positive (using the right-hand rule) about the x_1 -, y_1 -, and z_1 -axes, respectively. Note that the aerodynamic rolling moment whose output is depicted in Sample Page 9 is defined positive starboard side down and is opposite from the harmonically analyzed total rolling moment depicted in Sample Page 12. Sample Page 13 depicts the harmonic analysis of the flatwise stresses at the center of each of the spanwise segments. A similar output listing is provided for both edgewise and torsional stresses.

Sample Page 11

93

HARMONIC ANALYSIS OF HUB SHEARS AND MOMENTS

	AO	1	2	3	4	5	6	7	8	9	10
LONG. SMR	XX.X	XXXXX.X XXXXX.X XXXXX.X XXX.XX X.XX	XXX.X XXX.X XXX.X XXX.XX .XX	XXX.X XXX.X XXX.X XXX.XX .XX	XX.X XX.X XX.X XXX.XX .XX	XX.X XX.X XX.X XXX.XX .XX	XX.X XX.X XX.X XXX.XX .XX	XX.X XX.X XX.X XXX.XX .XX	XX.X XX.X XX.X XXX.XX .XX	XX.X XX.X XX.X XXX.XX .XX	XX.X XX.X XX.X XXX.XX .XX
LAT. SMR	XX.X	XXXXX.X XXXXX.X XXXXX.X XXX.XX X.XX	XXX.X XXX.X XXX.X XXX.XX .XX	XXX.X XXX.X XXX.X XXX.XX .XX	XX.X XX.X XX.X XXX.XX .XX	XX.X XX.X XX.X XXX.XX .XX	XX.X XX.X XX.X XXX.XX .XX	XX.X XX.X XX.X XXX.XX .XX	XX.X XX.X XX.X XXX.XX .XX	XX.X XX.X XX.X XXX.XX .XX	XX.X XX.X XX.X XXX.XX .XX
VERT. SMR	XX.X	XXXXX.X XXXXX.X XXXXX.X XXX.XX X.XX	XXX.X XXX.X XXX.X XXX.XX .XX	XXX.X XXX.X XXX.X XXX.XX .XX	XX.X XX.X XX.X XXX.XX .XX	XX.X XX.X XX.X XXX.XX .XX	XX.X XX.X XX.X XXX.XX .XX	XX.X XX.X XX.X XXX.XX .XX	XX.X XX.X XX.X XXX.XX .XX	XX.X XX.X XX.X XXX.XX .XX	XX.X XX.X XX.X XXX.XX .XX
ROLL MOMT	XX.X	XXXXX.X XXXXX.X XXXXX.X XXX.XX X.XX	XXX.X XXX.X XXX.X XXX.XX .XX	XXX.X XXX.X XXX.X XXX.XX .XX	XX.X XX.X XX.X XXX.XX .XX	XX.X XX.X XX.X XXX.XX .XX	XX.X XX.X XX.X XXX.XX .XX	XX.X XX.X XX.X XXX.XX .XX	XX.X XX.X XX.X XXX.XX .XX	XX.X XX.X XX.X XXX.XX .XX	XX.X XX.X XX.X XXX.XX .XX
PITCH MOMT	XX.X	XXXXX.X XXXXX.X XXXXX.X XXX.XX X.XX	XXX.X XXX.X XXX.X XXX.XX .XX	XXX.X XXX.X XXX.X XXX.XX .XX	XX.X XX.X XX.X XXX.XX .XX	XX.X XX.X XX.X XXX.XX .XX	XX.X XX.X XX.X XXX.XX .XX	XX.X XX.X XX.X XXX.XX .XX	XX.X XX.X XX.X XXX.XX .XX	XX.X XX.X XX.X XXX.XX .XX	XX.X XX.X XX.X XXX.XX .XX
YAW MOMT	XX.X	XXXXX.X XXXXX.X XXXXX.X XXX.XX X.XX	XXX.X XXX.X XXX.X XXX.XX .XX	XXX.X XXX.X XXX.X XXX.XX .XX	XX.X XX.X XX.X XXX.XX .XX	XX.X XX.X XX.X XXX.XX .XX	XX.X XX.X XX.X XXX.XX .XX	XX.X XX.X XX.X XXX.XX .XX	XX.X XX.X XX.X XXX.XX .XX	XX.X XX.X XX.X XXX.XX .XX	XX.X XX.X XX.X XXX.XX .XX

Impedance Matrices

When the analysis is optionally used to calculate impedance matrices (as controlled by input items 930 through 939, and 946) these matrices are output as shown in Sample Pages 14 and 15. Sample Page 14 presents the output format for the blade passage harmonic characteristics of conventionally defined hub loads and their respective impedances due to vibratory hub acceleration. The column denoted HUB LOADS presents the N/rev harmonic content of the hub loads as determined by summing contributions from all blades, where N is indicated in the first line of this sample page. Thus, the values in this column are equal to the Nth harmonic values shown in Sample Page 12 but multiplied by the number of blades. Note that, as shown in Sample Page 14, the results would be appropriate for the 4th harmonic hub loads for a four-bladed rotor. The columns denoted LDXC, LDYC, LDZC, LDXS, LDYS and LDZS present the derivatives of the respective HUB LOADS values with respect to N/rev vibratory displacements in the x, y and z directions, cosine and sine components each. The columns denoted RDXC, RDYC, ..., RDZS present similar derivatives of the hub loads with respect to vibratory rotations about the x, y and z axes, cosine and sine components each. Note that the units of the loads and perturbational quantities are defined in the second line of this sample page. The positive directions of the loads are also defined and are consistent with those of Sample Page 12.

Sample Page 15 presents elements of an "augmented" impedance matrix representing the partial derivatives of the HUB LOADS components, but with respect to the six components of higher harmonic (pitch) control angle (HHC) appropriate to N/rev vibratory hub loads. Normally these components consist of the cosine and sine components each of the N-1, N and N+1 harmonics. Note that Sample Page 15 indicates harmonic components of HHC appropriate to 4/rev vibrations. As indicated in the first line of this sample page the pitch angle perturbations have the units of degrees.

In Sample Page 16 is depicted the typical additional page of output generated at the beginning of every case following the first case of a multiple case sum. The two columns depict, respectively, the location numbers and data values for the newly inputted data distinguishing the present case from the previous one. This feature is intended solely as an ease of usage output to assist in data management.

SUMMARY OF ROTOR HUB 4/REV LOADS AND HUB IMPEDANCE MATRIX CALCULATIONS FOR 4/REV VIBRATORY HUB DISPLACEMENTS

UNITS... U(SHEAR) = LBS, U(MOMENT) = FT-LBS, U(LINEAR DISPLACEMENT) = FT, U(ROTATIONAL DISPLACEMENT) = RAD

CONVENTIONAL FOURIER SERIES REPRESENTATIONS

			HUB LOADS	LDXC	LDYC	LDZC	RDXC	RDYC	RDZC
LONG.	SHR (+, AFT)	COS	X.XXXE-YY	X.XXXE-YY	X.XXXE-YY	X.XXXE-YY	X.XXXE-YY	X.XXXE-YY	X.XXXE-YY
LAT.	SHR (+, STRBD)	COS	X.XXXE-YY	X.XXXE-YY	X.XXXE-YY	X.XXXE-YY	X.XXXE-YY	X.XXXE-YY	X.XXXE-YY
VERT.	SHR (+, UP)	COS	X.XXXE-YY	X.XXXE-YY	X.XXXE-YY	X.XXXE-YY	X.XXXE-YY	X.XXXE-YY	X.XXXE-YY
ROLL	MOMT (+, STRBD UP)	COS	X.XXXE-YY	X.XXXE-YY	X.XXXE-YY	X.XXXE-YY	X.XXXE-YY	X.XXXE-YY	X.XXXE-YY
PITCH	MOMT (+, NOSE UP)	COS	X.XXXE-YY	X.XXXE-YY	X.XXXE-YY	X.XXXE-YY	X.XXXE-YY	X.XXXE-YY	X.XXXE-YY
YAW	MOMT (+, OMEGA DIR.)	COS	X.XXXE-YY	X.XXXE-YY	X.XXXE-YY	X.XXXE-YY	X.XXXE-YY	X.XXXE-YY	X.XXXE-YY
LONG.	SHR (+, AFT)	SIN	X.XXXE-YY	X.XXXE-YY	X.XXXE-YY	X.XXXE-YY	X.XXXE-YY	X.XXXE-YY	X.XXXE-YY
LAT.	SHR (+, STRBD)	SIN	X.XXXE-YY	X.XXXE-YY	X.XXXE-YY	X.XXXE-YY	X.XXXE-YY	X.XXXE-YY	X.XXXE-YY
VERT.	SHR (+, UP)	SIN	X.XXXE-YY	X.XXXE-YY	X.XXXE-YY	X.XXXE-YY	X.XXXE-YY	X.XXXE-YY	X.XXXE-YY
ROLL	MOMT (+, STRBD UP)	SIN	X.XXXE-YY	X.XXXE-YY	X.XXXE-YY	X.XXXE-YY	X.XXXE-YY	X.XXXE-YY	X.XXXE-YY
PITCH	MOMT (+, NOSE UP)	SIN	X.XXXE-YY	X.XXXE-YY	X.XXXE-YY	X.XXXE-YY	X.XXXE-YY	X.XXXE-YY	X.XXXE-YY
YAW	MOMT (+, OMEGA DIR.)	SIN	X.XXXE-YY	X.XXXE-YY	X.XXXE-YY	X.XXXE-YY	X.XXXE-YY	X.XXXE-YY	X.XXXE-YY
				LDXS	LDYS	LDZS	RDXS	RDYS	RDZS
LONG.	SHR (+, AFT)	COS		X.XXXE-YY	X.XXXE-YY	X.XXXE-YY	X.XXXE-YY	X.XXXE-YY	X.XXXE-YY
LAT.	SHR (+, STRBD)	COS		X.XXXE-YY	X.XXXE-YY	X.XXXE-YY	X.XXXE-YY	X.XXXE-YY	X.XXXE-YY
VERT.	SHR (+, UP)	COS		X.XXXE-YY	X.XXXE-YY	X.XXXE-YY	X.XXXE-YY	X.XXXE-YY	X.XXXE-YY
ROLL	MOMT (+, STRBD UP)	COS		X.XXXE-YY	X.XXXE-YY	X.XXXE-YY	X.XXXE-YY	X.XXXE-YY	X.XXXE-YY
PITCH	MOMT (+, NOSE UP)	COS		X.XXXE-YY	X.XXXE-YY	X.XXXE-YY	X.XXXE-YY	X.XXXE-YY	X.XXXE-YY
YAW	MOMT (+, OMEGA DIR.)	COS		X.XXXE-YY	X.XXXE-YY	X.XXXE-YY	X.XXXE-YY	X.XXXE-YY	X.XXXE-YY
LONG.	SHR (+, AFT)	SIN		X.XXXE-YY	X.XXXE-YY	X.XXXE-YY	X.XXXE-YY	X.XXXE-YY	X.XXXE-YY
LAT.	SHR (+, STRBD)	SIN		X.XXXE-YY	X.XXXE-YY	X.XXXE-YY	X.XXXE-YY	X.XXXE-YY	X.XXXE-YY
VERT.	SHR (+, UP)	SIN		X.XXXE-YY	X.XXXE-YY	X.XXXE-YY	X.XXXE-YY	X.XXXE-YY	X.XXXE-YY
ROLL	MOMT (+, STRBD UP)	SIN		X.XXXE-YY	X.XXXE-YY	X.XXXE-YY	X.XXXE-YY	X.XXXE-YY	X.XXXE-YY
PITCH	MOMT (+, NOSE UP)	SIN		X.XXXE-YY	X.XXXE-YY	X.XXXE-YY	X.XXXE-YY	X.XXXE-YY	X.XXXE-YY
YAW	MOMT (+, OMEGA DIR.)	SIN		X.XXXE-YY	X.XXXE-YY	X.XXXE-YY	X.XXXE-YY	X.XXXE-YY	X.XXXE-YY

HUB IMPEDANCE MATRIX FOR HHC PITCH ANGLES (UNITS = DEG)

			A3S	A4S	A5S	B3S	B4S	B5S
LONG.	SHR (+, AFT)	COS	X.XXXE-YY	X.XXXE-YY	X.XXXE-YY	X.XXXE-YY	X.XXXE-YY	X.XXXE-YY
LAT.	SHR (+, STRBD)	COS	X.XXXE-YY	X.XXXE-YY	X.XXXE-YY	X.XXXE-YY	X.XXXE-YY	X.XXXE-YY
VERT.	SHR (+, UP)	COS	X.XXXE-YY	X.XXXE-YY	X.XXXE-YY	X.XXXE-YY	X.XXXE-YY	X.XXXE-YY
ROLL	MOMT (+, STRBD UP)	COS	X.XXXE-YY	X.XXXE-YY	X.XXXE-YY	X.XXXE-YY	X.XXXE-YY	X.XXXE-YY
PITCH	MOMT (+, NOSE UP)	COS	X.XXXE-YY	X.XXXE-YY	X.XXXE-YY	X.XXXE-YY	X.XXXE-YY	X.XXXE-YY
YAW	MOMT (+, OMEGA DIR.)	COS	X.XXXE-YY	X.XXXE-YY	X.XXXE-YY	X.XXXE-YY	X.XXXE-YY	X.XXXE-YY
LONG.	SHR (+, AFT)	SIN	X.XXXE-YY	X.XXXE-YY	X.XXXE-YY	X.XXXE-YY	X.XXXE-YY	X.XXXE-YY
LAT.	SHR (+, STRBD)	SIN	X.XXXE-YY	X.XXXE-YY	X.XXXE-YY	X.XXXE-YY	X.XXXE-YY	X.XXXE-YY
VERT.	SHR (+, UP)	SIN	X.XXXE-YY	X.XXXE-YY	X.XXXE-YY	X.XXXE-YY	X.XXXE-YY	X.XXXE-YY
ROLL	MOMT (+, STRBD UP)	SIN	X.XXXE-YY	X.XXXE-YY	X.XXXE-YY	X.XXXE-YY	X.XXXE-YY	X.XXXE-YY
PITCH	MOMT (+, NOSE UP)	SIN	X.XXXE-YY	X.XXXE-YY	X.XXXE-YY	X.XXXE-YY	X.XXXE-YY	X.XXXE-YY
YAW	MOMT (+, OMEGA DIR.)	SIN	X.XXXE-YY	X.XXXE-YY	X.XXXE-YY	X.XXXE-YY	X.XXXE-YY	X.XXXE-YY

Sample Page 15

PROGRAM G400 - CASE 2 OF A MULTI-CASE RUN. INPUT DATA REPRESENTING CHANGES TO THE PREVIOUS CASE ARE AS FOLLOWS:

[illegible]

Sample Page 16

REFERENCES

1. Bielawa, R. L.: Aeroelastic Analysis for Helicopter Rotor Blades with Time-Variable, Nonlinear Structural Twist and Multiple Structural Redundancy-Mathematical Derivation and Program User's Manual. NASA Contractor Report CR-2638, Oct. 1976.
2. Egolf, T. A. and A. J. Landgrebe: User's Manual for the UTRC Prescribed Wake Rotor Inflow and Flow Field Prediction Analysis.. United Technologies Research Center Report UTRC81-2, Jan. 1981.
3. Bisplinghoff, R. L., H. Ashley, and R. L. Halfman: Aeroelasticity. Addison-Wesley Publishing Co., Inc., Reading, MA., 1955, pp. 646-650.
4. Halfman, R. L.: Dynamics, Vol. I, Particles, Rigid Bodies, and Systems. Addison-Wesley Publishing Co., Inc., Reading, MA., 1962.
5. Heyson, H. H.: Linearized Theory of Wind-Tunnel Jet-Boundary Corrections and Ground Effect for VTOL-STOL Aircraft. NASA TR-124, 1962.
6. Hildebrand, F. B.: Introduction to Numerical Analysis. McGraw-Hill Book Co., Inc., New York, N.Y., 1956, pp. 429-434.
7. Bielawa, R. L.: Synthesized Unsteady Airfoil Data with Applications to Stall Flutter Calculations. American Helicopter Society, 31st Annual Forum Proceeding No. 935, May 1975.
8. Houbolt, J. C. and G. W. Brooks: Differential Equations of Motion for Combined Flapwise Bending, Chordwise Bending and Torsion of Twisted Nonuniform Rotor Blades. NASA Report 1346. October, 1956.

APPENDIX I

UPDATES TO DOCUMENTATION OF BASIC G400 ANALYSIS

Since the publication of Reference 1 the original G400 analysis has undergone continual development. In this process many of the original formulations and derivations have been reassessed, rechecked, and, where appropriate, reformulated. This appendix presents some of these reformulations and are, in fact, an errata update sheet to Reference 1.

1. The first such update pertains to the definitions for the deflection correction terms resulting from structural twist. In particular, the first order terms given by Eqs. (7) and (8) of Reference 1 should read, respectively, as:

$$\Delta v = \left[\int_0^{\bar{r}} \Theta' \gamma_{w_i} d\bar{r}_1 + \int_0^{\bar{r}} \int_0^{\bar{r}_1} \Theta' \gamma_{w_i} d\bar{r}_2 d\bar{r}_1 \right] q_{w_i} \quad (I.1)$$

$$\Delta w = \left[\int_0^{\bar{r}} \Theta' \gamma_{v_k} d\bar{r}_1 + \int_0^{\bar{r}} \int_0^{\bar{r}_1} \Theta' \gamma_{v_k} d\bar{r}_2 d\bar{r}_1 \right] q_{v_k} \quad (I.2)$$

2. The second update pertains to formulation of the elements of the inertia coupling matrix, [A], (Eq. (45) of Reference 1). This matrix should be completely symmetric; the offending terms, $A_{w_i \theta_j}$ and $A_{v_k \theta_j}$ should equal their respective transposed elements:

$$A_{w_i \theta_j} = A_{\theta_j w_i} = \int_0^1 m y_{10CG} \gamma_{\theta_j} (\gamma_{w_i} - \Delta w_i) dr \quad (I.3)$$

$$A_{v_k \theta_j} = A_{\theta_j v_k} = - \int_0^1 m y_{10CG} \gamma_{\theta_j} \Delta w_k dr \quad (I.4)$$

3. The third and fourth updates pertain to the implementation of the redundant analysis of flexbeam-torque tube assemblies. The first of these two relates to the torsional stiffness characteristics of the flexbeams. A more correct statement of the boundary conditions for the flexbeam torsion equation (Eq. (115) of Reference 1) includes relating the flexbeam outboard twist rate, $\Theta'(r_j)$, to the twist rate of the outer blade:

$$\Theta'(r_j) = \Theta'_j \quad (I.5)$$

where the twist rate of the outer blade comes from built-in and response contributions:

$$\Theta'_j = \Theta'_B(r_j) + \sum_{j=1}^{NTM} \gamma_{\theta_j}'(r_j) q_{\theta_j} \quad (I.6)$$

The inclusion of this generally nonzero value of twist rate has the effect of modifying the resulting expression for the elastic torsion deflection of the flexbeam at the juncture (Eq. (129a)):

$$\Delta \Theta_J = \frac{1}{(e_{11}e_{23} - e_{21}e_{13})} \sum_{i=1}^4 T_i [e_{13}(f_{2,i+1} + e_{22}\Theta'_J) - e_{23}(f_{1,i+1} + e_{12}\Theta'_J)] \quad (I.7)$$

and the symbolic expression for this deflection (Eq. (130b)) then becomes:

$$\begin{aligned} \Delta \Theta = & \theta_{sx} S_{x5_{FB}} + \theta_{Mx} M_{x5_{FB}} + \theta_{sy} S_{y5_{FB}} \\ & + \theta_{sz} S_{z5_{FB}} + \theta_{My} M_{y5_{FB}} + \theta_{Mz} M_{z5_{FB}} \\ & + \theta_{\theta}' \cdot \Theta'_J \end{aligned} \quad (I.8)$$

4. The fourth update pertains to the calculation of internal blade shears and moments in the blade adjacent to the juncture. As outlined in Reference 1 a force integration approach was implemented which necessitated extrapolations to estimate the modal accelerations. This calculation was found to be best performed using a mode deflection method instead. Thus, Eqs. (132b) and 132f) of Reference 1 are, respectively, replaced by the following expressions:

$$S_{y5_B} = -S \Theta_J \sum_{i=1}^{NFM} DS1_i q_{w_i} + c \Theta_J \sum_{k=1}^{NEM} DS3_k q_{v_k} \quad (I.9a)$$

$$S_{z5_B} = c \Theta_J \sum_{i=1}^{NFM} DS1_i q_{w_i} + s \Theta_J \sum_{k=1}^{NEM} DS3_k q_{v_k} \quad (I.9b)$$

$$M_{x5_B} = \sum_{j=1}^{NTM} DS5_j q_{\theta_j} \quad (I.9c)$$

$$M_{y_{5B}} = c \odot_j \sum_{i=1}^{NFM} DS2_i q_{w_i} - s \odot_j \sum_{k=1}^{NEM} DS4_k q_{v_k} \quad (I.9d)$$

$$M_{z_{5B}} = s \odot_j \sum_{i=1}^{NFM} DS2_i q_{w_i} + c \odot_j \sum_{k=1}^{NEM} DS4_k q_{v_k} \quad (I.9e)$$

where:

$$DS1_i = \omega_{w_i}^2 \int_{\bar{r}_j}^1 m \gamma_{w_i} d\bar{r} \quad (I.10a)$$

$$DS2_i = \int_{\bar{r}_j}^1 m \left[(\bar{r} - \bar{r}_j) \omega_{w_i}^2 \gamma_{w_i} - \bar{r} (\gamma_{w_i}(\bar{r}) - \gamma_{w_i}(\bar{r}_j)) \right] d\bar{r} \quad (I.10b)$$

$$DS3_k = (\omega_{v_k}^2 + 1) \int_{\bar{r}_j}^1 m \gamma_{v_k} d\bar{r} \quad (I.10c)$$

$$DS4_k = \int_{\bar{r}_j}^1 m \left[(\bar{r} - \bar{r}_j) (\omega_{v_k}^2 + 1) - \bar{r} (\gamma_{v_k}(\bar{r}) - \gamma_{v_k}(\bar{r}_j)) \right] d\bar{r} \quad (I.10d)$$

$$DS5_j = \int_{\bar{r}_j}^1 m \gamma_{\theta_j} \left[\omega_{\theta_j}^2 (\bar{k}_{z_{10}}^{-2} + \bar{k}_{y_{10}}^{-2}) + \bar{k}_{y_{10}}^2 - \bar{k}_{z_{10}}^2 \right] d\bar{r} \quad (I.10e)$$

1. Report No. NASA CR-165896		2. Government Accession No.		3. Recipient's Catalog No.	
4. Title and Subtitle Aeroelastic Analysis for Helicopter Rotors with Blade Appended Vibration Absorbers - Mathematical Derivations and Program User's Manual				5. Report Date June 1982	
				6. Performing Organization Code	
7. Author(s) R. L. Bielawa				8. Performing Organization Report No. UTRC81-45	
				10. Work Unit No.	
9. Performing Organization Name and Address United Technologies Research Center East Hartford, Connecticut 06108				11. Contract or Grant No. NAS1-16058	
				13. Type of Report and Period Covered Contractor Report	
12. Sponsoring Agency Name and Address National Aeronautics and Space Administration Langley Research Center, Hampton, VA 23665				14. Sponsoring Agency Code	
15. Supplementary Notes Langley technical monitor: Robert Tomaine Final Report					
16. Abstract <p>Mathematical development is presented for the expanded capabilities of the United Technologies Research Center (UTRC) G400 Rotor Aeroelastic Analysis. This expanded analysis, G400PA, simulates the dynamics of teetered rotors, blade pendulum vibration absorbers and the higher harmonic excitations resulting from prescribed vibratory hub motions and higher harmonic blade pitch control. Formulations are also presented for calculating the rotor impedance matrix appropriate to these higher harmonic blade excitations. This impedance matrix and the associated vibratory hub loads are intended as the rotor dynamic characteristics elements for use in the Simplified Coupled Rotor/Fuselage Vibration Analysis (SIMVIB).</p> <p>Sections are included presenting updates to the development of the original G400 theory, and material appropriate to the user of the G400PA computer program. This material includes (1) a general description of the structuring of the G400PA FORTRAN coding, (2) a detailed description of the required input data and other useful information for successfully running the program, and (3) a detailed description of the output results.</p>					
17. Key Words (Suggested by Author(s)) Rotor Aeroelasticity Vibration Higher Harmonic Control Vibration Absorber Teetered Rotors			18. Distribution Statement Unclassified - Unlimited		
19. Security Classif. (of this report) Unclassified	20. Security Classif. (of this page) Unclassified	21. No. of Pages 103	22. Price		

End of Document